AD-A085 866 EATON CORP DEER PARK NY AIL DIV F/G 17/9
ANALYSES FOR MULTISTATIC GEOMETRIC IMAGE CORRECTION.(U)
FEB 80 J S PRICHARD, R A BAKER, W J CAPITI F30602-79-C-0137
UNCLASSIFIED E034-1 RADC-TR-80-18 NL

END
DATE FILMED
8-80
DTIC

RADC-TR-80-18
Final Technical Report
February 1980

ANALYSES FOR MULTISTATIC GEOMETRIC IMAGE CORRECTION

Eaton Corporation

J. S. Prichard
R. A. Baker
W. J. Capiti

ROME AIR DEVELOPMENT CENTER
Air Force Systems Command
Griffiss Air Force Base, New York 13441

This report has been reviewed by the RADC Public Affairs Office (PA) and is releasable to the National Technical Information Service (NTIS). At NTIS it will be releasable to the general public, including foreign nations.

RADC-TR-80-18 has been reviewed and is approved for publication.

APPROVED: Daniel L. Tauroney

DANIEL L. TAURONEY
Project Engineer

APPROVED: Frank J. Rehm

FRANK J. REHM
Technical Director
Surveillance Division

FOR THE COMMANDER: John P. Huss

JOHN P. HUSS
Acting Chief, Plans Office

If your address has changed or if you wish to be removed from the RADC mailing list, or if the addressee is no longer employed by your organization, please notify RADC (OCTM), Griffiss AFB NY 13441. This will assist us in maintaining a current mailing list.

Do not return this copy. Retain or destroy.

UNCLASSIFIED

SECURITY CLASSIFICATION OF THIS PAGE (When Data Entered)

REPORT DOCUMENTATION PAGE	READ INSTRUCTIONS BEFORE COMPLETING FORM
1. REPORT NUMBER: RADC-TR-80-18	2. GOVT ACCESSION NO.: AD-A085866
3. RECIPIENT'S CATALOG NUMBER:	
4. TITLE (and Subtitle): ANALYSES FOR MULTISTATIC GEOMETRIC IMAGE CORRECTION.	5. TYPE OF REPORT & PERIOD COVERED: Final Technical Report. 18 Apr — 19 Oct 79.
	6. PERFORMING ORG. REPORT NUMBER: E934-1
7. AUTHOR(s): J. S. Prichard, R. A. Baker, W. J. Capiti	8. CONTRACT OR GRANT NUMBER(s): F30602-79-C-0137
9. PERFORMING ORGANIZATION NAME AND ADDRESS: Eaton Corporation, AIL Division, Comac Road, Deer Park NY 11729	10. PROGRAM ELEMENT, PROJECT, TASK AREA & WORK UNIT NUMBERS: 61102F, 23050908, J9
11. CONTROLLING OFFICE NAME AND ADDRESS: Rome Air Development Center (OCTM), Griffiss AFB NY 13441	12. REPORT DATE: February 1980; 13. NUMBER OF PAGES: 71
14. MONITORING AGENCY NAME & ADDRESS (if different from Controlling Office): Same	15. SECURITY CLASS. (of this report): UNCLASSIFIED; 15a. DECLASSIFICATION/DOWNGRADING SCHEDULE: N/A

16. DISTRIBUTION STATEMENT (of this Report)

Approved for public release; distribution unlimited.

17. DISTRIBUTION STATEMENT (of the abstract entered in Block 20, if different from Report)

Same

18. SUPPLEMENTARY NOTES

RADC Project Engineer: Daniel L. Tauroney

19. KEY WORDS (Continue on reverse side if necessary and identify by block number)

Synthetic aperture radar (SAR)	Bistatic synthetic aperture radar
Stretch radar	Multistatic radar
Spotlight radar	Multistatic synthetic aperture radar
High resolution radar	Radar imagery
Bistatic radar	Image processing
	Image correction

20. ABSTRACT (Continue on reverse side if necessary and identify by block number)

Polar format storage of two-dimensional monostatic synthetic aperture radar (SAR) data (gathered in the stretch-spotlight mode of operation) allows matched two-dimensional Fourier transform processing; it eliminates range walk, allowing maximum size field of view for a given resolution or finest resolution for a given size field of view.

(Cont'd)

DD FORM 1 JAN 73 1473 EDITION OF 1 NOV 65 IS OBSOLETE

UNCLASSIFIED

SECURITY CLASSIFICATION OF THIS PAGE (When Data Entered)

404967

Item 20 (Cont'd)

In a bistatic SAR system, iso-range and iso-Doppler contours are orthogonal only for zero bistatic angle. The range gradient diminishes as the bistatic angle is increased. When polar format storage is used, these effects result in increasing smearing (defocusing) and geometric distortion of the imagery as the bistatic angle is increased. Hence, such formatting is not matched to two-dimensional transform processing.

A solution to the bistatic SAR image processing problem is provided by a new technique called coherent unskewing and reconstitution logic (Curl). The matched processing performance of the Curl technique is demonstrated using computer simulation of received data from a bistatic SAR system with two-dimensional geometry. The resulting imagery is sharply focused and is totally free of geometric distortion.

With three-dimensional system geometry, the use of Curl with two-dimensional data storage and processing (with a fixed data storage plane corresponding to the synthetic aperture center) may provide a projected image with acceptably small distortion. Tradeoff curves are given for estimating the orientation of the projection plane as a function of system geometry and other pertinent parameters.

TABLE OF CONTENTS

LIST OF ILLUSTRATIONS

EVALUATION

Airborne Instruments Lab (AIL) was successful in removing radar image distortion for bistatic radar configuration. They demonstrated a technique which records data in such a way as to remove the "doppler walk" through resolution cells when generating an image from radar data. This technique will have application in tactical target identification when the target is being imaged by more than one radar and will reduce the amount of aspect angle change, or time on target, frequently required. This effort is related to TPO R2E.

DANIEL L. TAURONEY
Project Engineer

1. INTRODUCTION

Bistatic, or, more generally, multistatic radar has certain advantages compared to monostatic radar. A key advantage is the added security it provides to the receiving platform in the modern electronic warfare environment. (By eliminating the transmission of electromagnetic energy, either completely or at least in the direction of the target area, its vulnerability to antiradiation missiles (ARM's) is essentially eliminated.) Another advantage is improved target signature quality because of the multiple aspect angles observed. However, the various advantages are bought at the cost of generally increased complexity of the multistatic radar system.

Fine resolution synthetic-aperture radar (SAR) imagery is a potential means of obtaining target classification and identification. For monostatic SAR, the polar format method of processing data from a spotlight radar avoids the problem of range walk, thereby facilitating the obtaining of fine resolution over a usefully large area. For bistatic SAR, however, the nonorthogonality of the lines of constant range and constant Doppler does not permit comparable results with polar format processing, unless the transmitter and receiver are nearly collinear from the target area (that is, when the bistatic angle is very small). A means for achieving the appropriate data formatting has been devised by AIL. The method is referred to as Coherent Unskewing and Reconstituting Logic (Curl).

The processing technique has been recently demonstrated under an IR&D program, using optical data recording and processing techniques (by additions and modifications to AIL's Mini-Spotlite radar data recording and processing equipment). The objective of the program reported herein was to extend the techniques to provide digital processing solutions both for the case where the transmitter and receiver are in the same plane as the field of view and for the more general case where they are not in the plane of the field of view.

The processing solutions for the two-dimensional case are demonstrated on small digital arrays of synthetically generated bistatic radar data, using a synthetic aircraft target consisting of a small number of point targets. The Curl processing demonstrates the formation of well-focused imagery, exhibiting fine resolution, low side lobes, and freedom from geometric distortion. The limitation on these aspects of the radar imagery have been found to be equivalent to those for monostatic radar imagery with comparable radar and geometric parameters, when using polar format processing. That is, insofar as processing limitations are concerned, if sufficient transmitted bandwidth and angular aperture is available, Curl processing can provide imagery that is fully the equivalent of that provided by polar format processing of monostatic radar data. However, it must be recognized that there are important other differences in a practical radar system. In particular, target properties (such as the bistatic radar cross section compared to the monostatic radar cross section and bistatic shielding compared to monostatic shielding) will generally result in imagery differences that are unrelated to the processing algorithms used. Further, in actual SAR systems, the increased transmitted bandwidth necessary to support a specified range resolution, as bistatic angle is increased, may be impractical or unaffordable. Similarly, where only the transmitter or receiver has tangential motion with respect to the target, such tangential motion provides a synthetic aperture only half that in the corresponding monostatic case. Thus, while Curl processing provides an elegant and exact solution to the processing of synthetic aperture data from two-dimensional bistatic radar system geometries, it is not a panacea for the other difficulties of bistatic synthetic aperture radar.

With respect to the general three-dimensional bistatic SAR geometry, where the departure from the two-dimensional case is slight, use of an imaging plane that represents the average or midposition over the synthetic aperture provides a convenient practical solution with little distortion.

Analysis of the three-dimensional bistatic geometry has led to expressions for the orientation of the image projection plane. From these generalized expressions a series of tradeoff curves have been calculated. The curves can be used to aid in the selection of transmitter and receiver site geometry or, in a multistatic synthetic aperture radar system, to select the most advantageous transmitter/receiver combinations for a given engagement.

The report concludes with a discussion of additional investigations that could lead to determining image distortion and resolution limits and also verifying improved means for reducing image distortion.

2. CURL PROCESSING FOR TWO-DIMENSIONAL CASE

2.1 GEOMETRY AND CURL STORAGE EQUATIONS

A detailed discussion and derivation of the Curl processing concept is contained in a proprietary AIL Technical Note, "Curl Image Processing for Bistatic Imaging Radar," J-D739, July 1978.

2.2 COMPUTER SIMULATION OF TWO-DIMENSIONAL BISTATIC SAR OPERATION

2.2.1 Operation Simulated

The generalized two-dimensional bistatic SAR geometry to be simulated is shown in Figure 1A. Basic assumptions are made that are analogous to those used in the polar processing of monostatic SAR data:

- The geometry is planar, with the image plane determined by the transmitter, receiver and center of the field of view.
- The transmitter and receiver are both sufficiently remote from the field of view that their direction from any point in the field of view is constant at any instant of time. Thus, the differential range of any target component from the reference point is measured along the line from the transmitter (or receiver) passing through the reference point to the perpendicular projection of the target point on that line (as shown in Figure 1A).

The normal operation of a high resolution synthetic aperture radar with digital data recording and processing equipments, when imaging a target area, would proceed as follows:

- Recording
  - For each transmitted pulse the received coherent video data would be quadrature sampled at a fixed rate.
  - The received quadrature video data samples would be digitized and recorded on magnetic tape.
  - The set of samples received from each particular transmitted pulse would be identified in some manner for later use in data processing. (Normally, the identification would be by time; however, target position or other quantities relatable to the data storage angle could also be used.)

  Image Processing

  - The recorded data would be reformatted (from the form in which it was recorded) to a rectilinear form suitable for application of a two-dimensional Fourier transform. This conversion could be performed in one of two ways:
    - For each point in the rectilinear data array, data would be selected from the nearest corresponding point in the original data array. If the original data were sufficiently oversampled, the resulting errors (of data at the nearest neighbor compared to at the exact point desired) would be negligible.
    - For each point in the rectilinear data array, data would be interpolated (normally in two dimensions) using the original data array.
  - The rectilinear data would be Fourier transform processed in the two orthogonal directions (after weighting, if desired, for reduction of side lobe levels) to form an image of the target area.

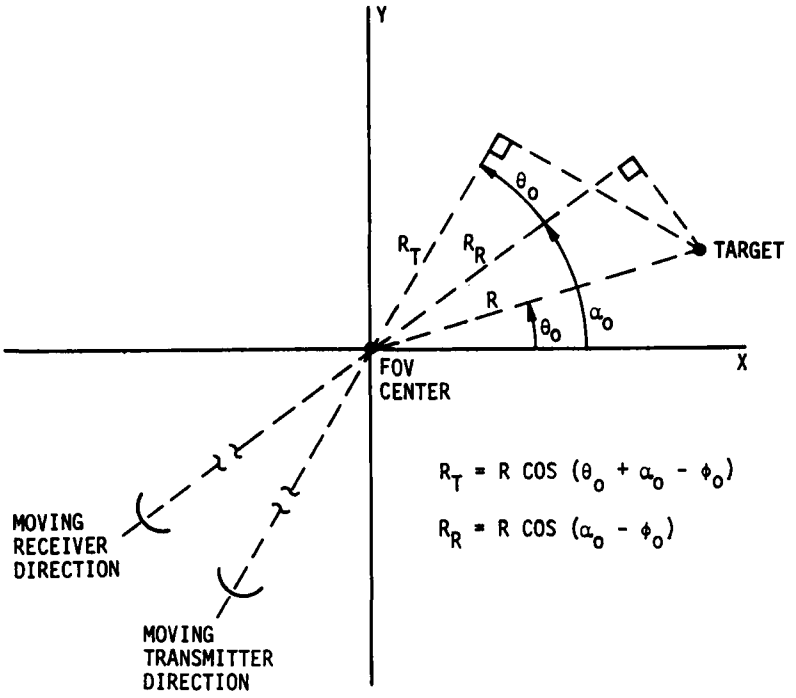

A. GENERALIZED TWO-DIMENSIONAL BISTATIC GEOMETRY

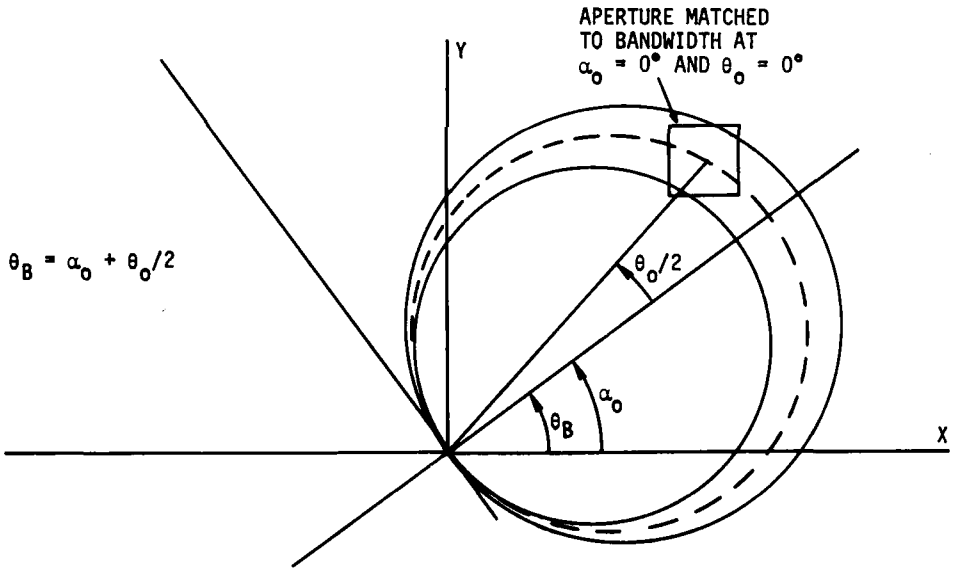

B. CURL STORAGE SURFACE

9-2476

Figure 1. Generalized Two-Dimensional Bistatic Geometry and Curl Storage Surface

2.2.2 Computer Simulation Description

For the purpose of these demonstrations of the quality of imagery obtainable using the Curl bistatic processing process, computer simulation of the received video signal will be used. This is in lieu of using a real bistatic radar system in flight or on a test range.

Instead of assigning some particular motion of the transmitter, receiver, and target as a function of time, for simulation purposes it is convenient to effectively work the problem backwards. That is, the rectilinear data array is filled (in some convenient order) by determining the bistatic angle, bisector direction, and (fast) time corresponding to each data array point. Then the direction to the transmitter and receiver are determined to match this condition. For convenience in the simulation (and to correspond to the condition specified in the Statement of Work) the receiver (or transmitter) is fixed in direction (that is, has no tangential velocity, but may have radial velocity with respect to the target). Then the moving transmitter (or receiver) direction changes at twice the rate of the bistatic angle bisector direction change. By the use of this backward approach, only the desired set of rectilinearly formatted data is obtained. Thus, the problem of data interpolation and its possible errors are avoided in this simulation.

The bistatic SAR input data (complex coherent video data samples) are simulated by the following steps for each target point:

- For θ_B, the selected transmitter angle at the center of the synthetic aperture (corresponding to the center of the array in which the simulated data is stored), determine the X and Y offset components of the center of the simulated data array from its non-offset position [corresponding to the selected reference point location (X_R, Y_R)].
- Determine $\emptyset_o$ for target point.
- Determine θ_o for initial point in data array (X = 1, Y = 1), using fixed α_o and $\emptyset_o$.
- Determine T for $\theta_{o/2}$ (half bistatic angle).
- Determine transmitter and receiver range component from reference to target point. These are R cos $(\theta_o + \alpha_o - \emptyset_o)$ and R cos $(\alpha_o - \emptyset_o)$, respectively, where R is the radial range of the target point from the reference point.
- Determine range frequency and phase.
- Determine quadrature components of signal at initial data point.
- Add quadrature components of any other target at initial data point.
- Determine quadrature components of signal for all other points by appropriately incrementing both X and Y over the range 1 to N (where N = number of data points on each side of the signal data array).

In order to scale the computer simulated data, the simulation program includes the following parameters (fixed for a given version of the program).

- Start frequency of FM waveform
- End frequency of FM waveform
- Duration of FM waveform
- Resolution (separation of image array points)

For a given simulation run, the following parameters are input from the computer terminal keyboard:

- Fixed receiver (or transmitter) angle

- Transmitter (or receiver) angle at center of the synthetic aperture
- Target coordinates (X, Y)

The overall base program for simulating bistatic radar data and applying Curl processing performs the following functions in the order given:

- Prints program name and characterization
- Loads complex data array with zeros to ensure no carry over of unwanted prior data
- Accepts keyboard input of receiver angle (α_0), in degrees
- Accepts keyboard input of transmitter center angle (θ_B), in degrees
- Accepts keyboard input of target coordinates (X, Y), in pixels
- Loads data array with simulated target return data in complex form by calculating transmitter angle and range delay that correspond to each data array point using Curl storage equations
- Accepts keyboard input for additional target coordinates and adds target data to data array until no further targets are desired
- Optionally, prints input data array (as 0 or blank, corresponding to ≤ 0 and > 0, respectively)
- Hamming weights and FFT's data array first in range dimension, then in azimuth dimension
- Prints maximum amplitude (in dB, reference 1) of output data array
- Prints quantized amplitude of output data array (coded "#" for maximum amplitude to -0.3 dB, coded "9" to "0" for 10 successive 3 dB ranges, and coded "blank" for -30.3 dB and lower amplitudes)

A number of modified versions of this program have been created for producing the several related plots presented. These include provisions for:

- Loading a simulated aircraft target that is stored in memory as eight equal-amplitude point target components (in place of manual keyboard entry of one or more target points). (Output plots use only the symbols "#", "9", "8", "7", and "6" to avoid image confusion by including the lower amplitude levels.)
- Processing with polar processing algorithm, rather than Curl algorithm.
- Processing with reduced transmitting bandwidth fixed at a multiple (such as 2) of that necessary to obtain the desired resolution at zero bistatic angle, rather than sufficiently wide to support the desired resolution to any specified bistatic angle.
- Simulating fixed bistatic angle operation, rather than holding either receiver or transmitter angle fixed while the other angle is varied (producing variable bistatic angle operation).

2.2.3 Computer Generated Plot Formats

Two types of computer-generated illustrations are used to demonstrate the two-dimensional bistatic data processing. These are described in turn.

2.2.3.1 Output Data Printout-This is a computer-generated plot of the image of the simulated target obtained by a two-dimensional Fourier transform of the input data. A (nearly) square array of 32 × 32 data points is plotted; 12 levels of amplitude are displayed. The largest magnitude point on a given plot and all others within 0.3 dB of that magnitude are plotted as "#". The magnitudes at all other

points are quantized into 3-dB bands and plotted as the characters "9" through "0" and "blank" (more than 30.3 dB below the maximum value). To facilitate determining the coordinates of any points, scales (in pixels) surround the output image plot. Note that the orientation of the data array is fixed and corresponds to viewing the scene from below the printout, that is at an angle of 90 degrees as defined in Figure 1A. With proper processing the image should be invarient with any transmitter and receiver angles. This fixed orientation of the field of view was chosen for these demonstrations to facilitate detection of any image distortion when the transmitter and/or receiver aspect angle is changed.

For all of the output printouts presented, the receiver angle is 0 degree and the transmitter angles are varied from 0 degree, typically in 45-degree increments, to 180 degrees. Because there is mirror symmetry of the images for the range of transmitter angles from 360 down to 180 degrees to those of in the range of 0 to 180 degrees, only the latter range is presented. Because the receiver is fixed at 0 degree, the bistatic angle is equal to the transmitter angle for all the images presented.

2.2.3.2 Input Array Printout-This is a computer-generated plot of the data array used to explain the phenomenon of range resolution being dependent on bistatic angle for finite transmitted bandwidth. The plot is a (nearly) square array of 32 × 32 points. These points are coded "blank" to represent normal input data; they are coded "0" to represent the absence of input data. The latter results from the range scale variation applied to the input data (by the Curl algorithm) to compensate for the reduction in range gradient as the bistatic angle is increased.

2.2.4 Simulated Imagery for Various Processing Algorithms and Motions

2.2.4.1 Curl Processing--Extremely Wide Transmitted Bandwidth-The effectiveness of Curl processing will be demonstrated first for the general case where the transmitter and receiver effectively rotate about the target at different rates. Without loss in generality, the simulation actually assumes that the net effective rotation rate of either the receiver (as suggested in the Statement of Work) or the transmitter is zero. As a further simplification, for this first case, it is assumed that the transmitted bandwidth can be made as wide as is necessary to support the desired range resolution to any specified bistatic angle less than 180 degrees.

For this case it can be seen from Figure 2 that for all combinations of transmitter and receiver angles (and the resulting bistatic angles selected) the resulting imagery is:

- Totally free of geometric distortion (all dimensions are faithfully preserved).
- Sharply focused, with fixed resolution determined by system parameters, including fixed data aperture size, independent of transmitter and receiver angles (and the resulting bistatic angles).

It might be expected that in Figure 2G, where the bistatic angle is 180 degrees (at the center of the synthetic aperture) the image would be smeared in the horizontal (X) direction. This would be the case at exactly 180 degrees, as the range gradient is then zero. However, for the parameters chosen for this series of Figures, the synthetic aperture is about 3 degrees. This fact, coupled with the extremely large bandwidth used, results in an image at a bistatic angle of 180 degrees that is nearly identical to that obtained at all smaller bistatic angles.

2.2.4.2 Curl Processing--Matched Transmitted Bandwidth-Next, the practical application of Curl will be demonstrated. In general, the transmitted bandwidth cannot be made as wide as assumed in the first case. Instead, a narrower transmitted bandwidth would be used, adequate to support a specific resolution at some bistatic angle that is appreciable less than 180 degrees. Then, using a fixed data aperture, constant resolution, of the specified value, is obtained at all smaller bistatic angles. Alternatively, by using a variable data aperture that is matched to the available data extent at each different bistatic angle, the system resolution becomes finer than the design point value at smaller bistatic angles. The system resolution will become coarser at bistatic angles greater than the design point value. Note that this coarsening of the resolution is not a defect of the Curl processing; it is the inevitable result of the bistatic geometry itself. This variation of the iso-range contour gradient is compensated by the Curl processing algorithm, thereby eliminating the geometric

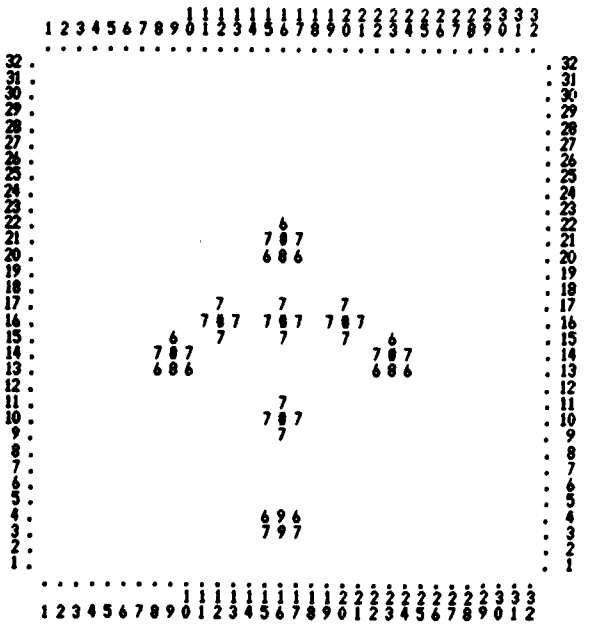

A. $\theta_0 = 0°$

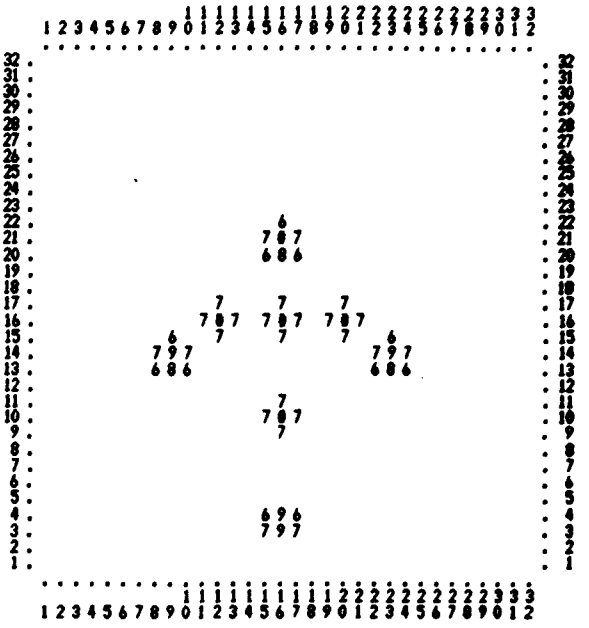

B. $\theta_0 = 45°$

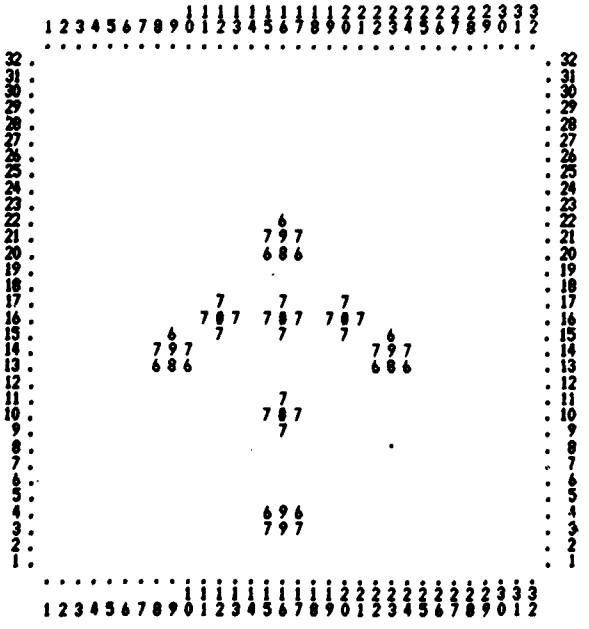

E. $\theta_0 = 170°$

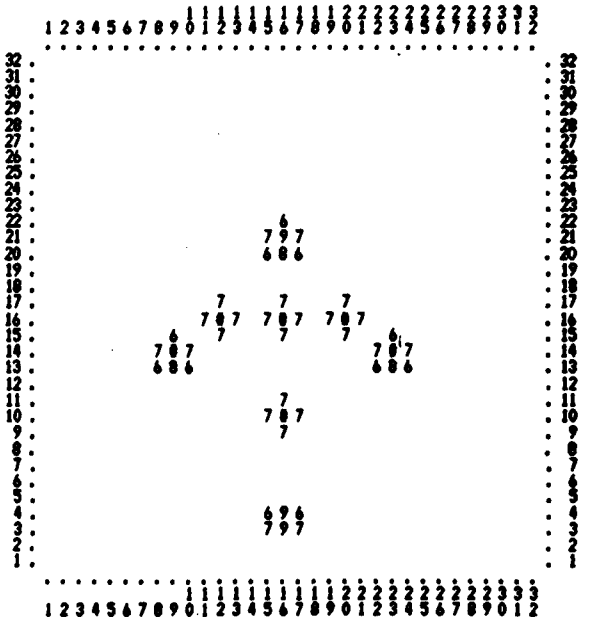

F. $\theta_0 = 175°$

9-2477

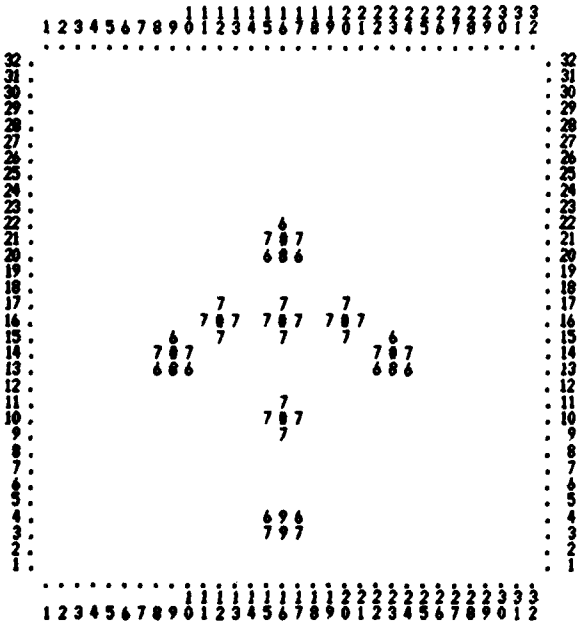

C. $\theta_0 = 90°$

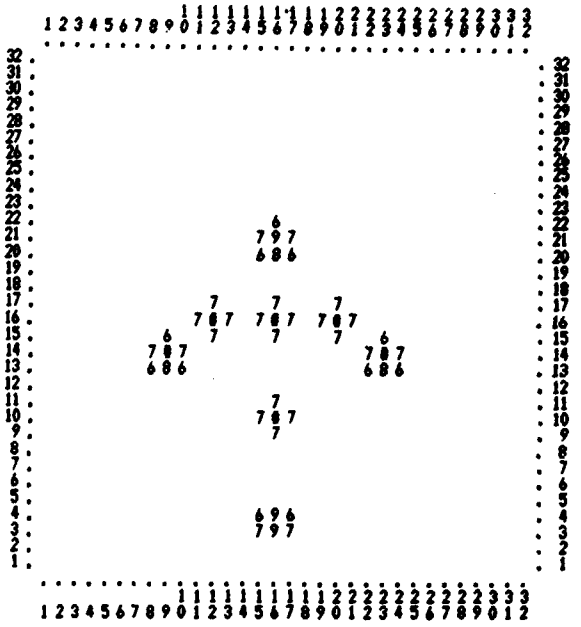

D. $\theta_0 = 135°$

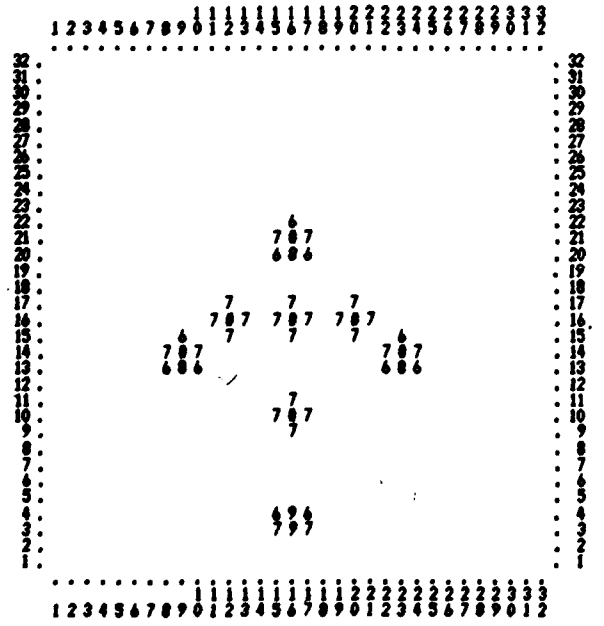

G. $\theta_0 = 180°$

Figure 2. Simulated Aircraft Image--Curl Processi Bandwidth Factor Very Large

2

distortion that would otherwise occur (as is shown in the following section when polar format processing, rather than Curl processing, is used). However, this also reduces the fast-time extent of the data relative to the data array (processing aperture). When the data extent becomes less than the aperture dimension the range resolution is correspondingly coarsened.

To demonstrate this situation, the transmitted bandwidth that is chosen is just twice that required to support the specified resolution under the most favorable condition of zero bistatic angle. Then, at bistatic angles greater than a specific value (45 degrees in this case), the available data does not fully fill the data array (processing aperture) and the resolution is consequently reduced.

For this matched bandwidth case it can be seen from Figure 3 that, for all combinations of transmitter and receiver angles selected, the resulting imagery is:

- Totally free of geometric distortion and properly located within the field of view.
- Sharply focused with resolution becoming less fine as the bistatic angle increases beyond some specific value (determined by the chosen excess bandwidth factor).

Note that Figures 3A, B and C are essentially identical to the corresponding Figures 2A, B, and C for bistatic angles of 0, 45, and 90 degrees, respectively. However, Figure 3D (bistatic angle of 135 degrees) is noticeably smeared in the now-diagonal range direction. This is a direct result of the greatly reduced range gradient at 135 degrees compared to 0 degree. Similarly, Figure 3E (bistatic angle of 150 degrees) is further smeared in the range direction.

The reasons for the reduced range resolution as the bistatic angle is increased are shown in Figures 4 and 5. Figure 4 shows the Curl data storage surface for the cases corresponding to Figure 3. With the chosen bandwidth factor of 2 the processing aperture is filled at bistatic angles of 0 and 45 degrees. However, at bistatic angles of 90, 135, and 150 degrees, the aperture is less than fully filled. These cases are more clearly illustrated in Figure 5, which shows the processing aperture (data array) for those cases (θ = 90, 135, and 150 degrees) illustrated in Figure 3 where the processing aperture is less than completely filled. Notice that, while at 90 degrees the aperture is nearly filled, as the bistatic angle is increased the aperture becomes less filled. (At 90 degrees 38 of the total 1024 data points in the array are unfilled; with data at 135 degrees 654 are unfilled; while at 150 degrees 869 are unfilled.

If a specified range resolution is desired at a specified bistatic angle it is possible to provide it by appropriate choice of the bandwidth factor. Thus, to a bistatic angle of almost 90 degrees, a bandwidth factor of 2 is sufficient. If this performance is desired to a bistatic angle of 135 degrees, for example, then a bandwidth factor of about 10 is required. Figure 6 shows the desired performance; no coarsening of resolution to 135 degrees, and slow coarsening of resolution at bistatic angles greater than 135 degrees. Note, however, that at 145 degrees, with 146 of 1024 data points unfilled, the resolution coarsening is almost imperceptable. At 155 degrees, with roughly half the data points unfilled (495 of 1024), the resolution is about half the initial resolution.

2.2.4.3 Polar Processing of Rotating Target (Fixed Bistatic Angle) Bistatic Data-For the special case in which the target rotates, or equivalently when transmitter and receiver rotate about the target at equal rates, the bistatic angle remains constant. For this case,

polar processing* suffices to produce an image that appears undistorted in shape, but is reduced in linear scale and displacement from the reference point. The image, however, is otherwise undistorted in that the scale change is the same in the orthogonal directions; hence, all angles are preserved. Thus, if scale is disregarded or corrected, aircraft recognition would be unimpeded. Since scale would appear to be an important ingredient in aircraft recognition algorithms, it would appear desirable to provide scale factor correction to the image or in the processing. (This is an inherent part of the Curl processing algorithm.)

Figure 7 shows polar processed rotating-target imagery, without scale factor correction. Note that, in general, the symmetrically located target points are represented by somewhat different clusters of numbers (representing amplitude of response). This is simply the result of the coarse quantization used and the fact that the sampling points are not symmetrically located on the amplitude response function. Actually, the image is free of any distortion except for the scale factor. When the data are stored prior to Fourier transform processing in such a way as to correct the scale factor, the resulting imagery is identical to that of Figure 2 for Curl processing. In both cases, the transmitted bandwidth is extremely wide so that no significant coarsening of the resolution is apparent as the bistatic angle is increased.

2.2.4.4 Polar Processing of Variable Bistatic Angle Data-The foregoing section demonstrated the imagery resulting from the special case of fixed bistatic angle. For this case bistatic polar processing produced images having perfect shape but incorrect scale.

Next to be considered is the general case in which the bistatic angle is varied during the synthetic aperture. Before presenting the imagery of the simulated aircraft used to demonstrate the prior cases it is instructive to show the imaging of a single point target. This is illustrated in Figure 8. Figure 8A is the locus of a target point at X = 24 pixels and Y = 0 pixels. In the upper plot the locus is shown in a single 32 × 32 pixel field of view. In the lower plot the locus is shown "unfolded" in two adjacent field-of-view areas to more clearly illustrate the typical form of the locus--a roughly triangular shape with the sides generally curved lines that form cusps at the vertices of the "triangle." In both plots, the number adjacent to each plotted point is the transmitter angle, which is shown (generally in 15-degree increments) from 0 to 360 degrees. For other values of X the locus is similarly shaped and scaled so that, at a transmitter angle of 0 degree, the target point images at the correct location in the field of view.

Similarly, Figure 8B is for a target point at X = 0 pixels and Y = 24 pixels. (In this case the third side is a straight line corresponding to the transmitter angle of 180 degrees; in Figure 8A the third side was a curved line and 180 degrees was represented by a single point on the locus.) Also correspondingly, for other values of Y, the locus is similarly shaped and scaled so that at 0 degree the target images at the correct location.

Figure 8C, for X=24 pixels and Y = 24 pixels, illustrates the more general case where neither X nor Y is zero. While the general cusped triangle shape is preserved, the locus is no longer symmetrical as were the prior cases (about the axis on which the target point was located). For this case, if the X, Y coordinates of the target point are scaled by the same factor, the locus is similarly shaped and appropriately scaled so that it passes through the correct location when the transmitter angle is zero.

---

*Polar processing is here defined by angular data storage equal to bistatic bisector angle and linear range storage, as in monostatic polar processing.

The significant point illustrated by Figure 8 is that, while there are gross similarities in the shapes of the loci when plotted in the "unfolded" format, there are also very significant differences. In general, the loci for target points at different locations within the field of view are sufficiently different that clearly apparent distortion of the image shape occurs for multipoint targets. This is illustrated in Figure 9 for the same simulated aircraft target used previously. Note that for zero bistatic angle no distortion is apparent, while at 45 degrees bistatic angle the distortion is quite apparent. At larger bistatic angles the distortion is sufficiently severe that aircraft recognition is severely impeded or made totally impractical.

The use of simple polar processing (as opposed to the matched processing of Curl) leads to a further difficulty not readily apparent in Figure 9. In addition to distortion of the images, displacement of the image within the field of view also occurs. To facilitate observation of the image distortion, all images of Figure 9, except that of Figure 9A for zero bistatic angle, have been offset (by interger numbers of pixels) in both the X and Y directions so as to approximately center the simulated aircraft image. These offsets are shown on each image subtitle. Thus, it is seen that, in general, for polar processing not only is the image distorted in shape and scale but it is improperly located within the field of view as well, further compounding the problem of aircraft recognition.

Because of the complex form of the image distortion and position error, it appears impractical to apply a transformation that would correct these imaging errors after the image is formed. However, as was demonstrated in Figures 2, 3, and 6, the use of the Curl algorithm to properly store the data prior to image formation easily removes the cause of the image distortion and position error and results in properly located and undistorted imagery.

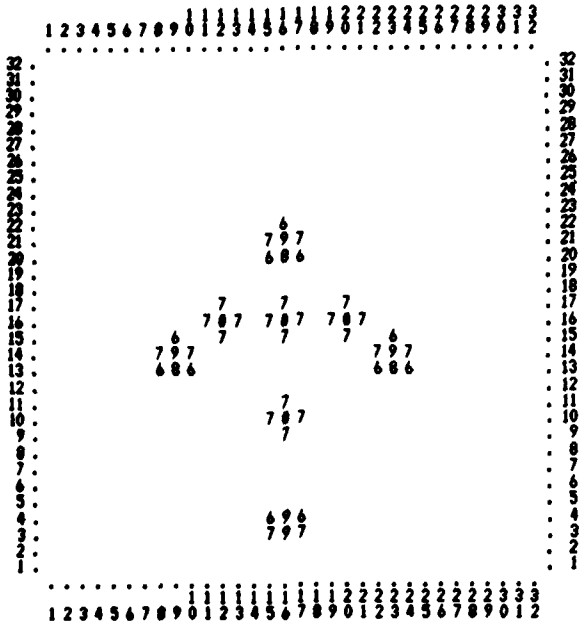

A. $\theta_0 = 0°$

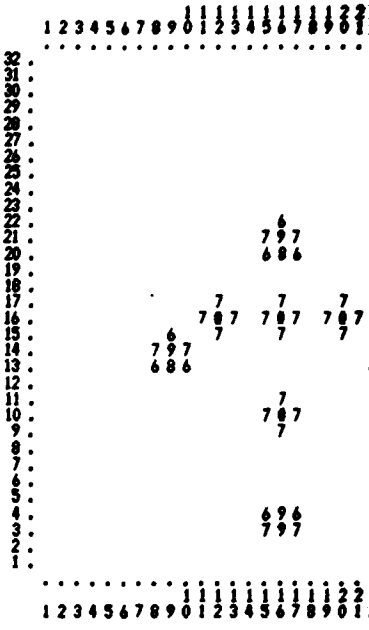

B. $\theta_0 = 45°$

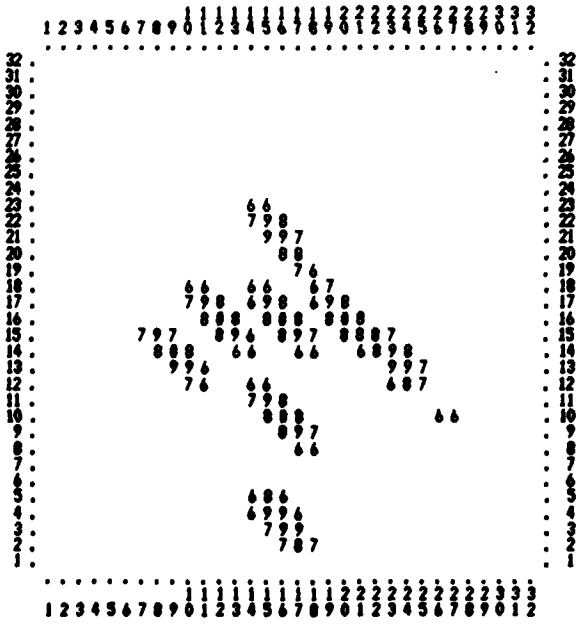

D. $\theta_0 = 135°$

9-2478

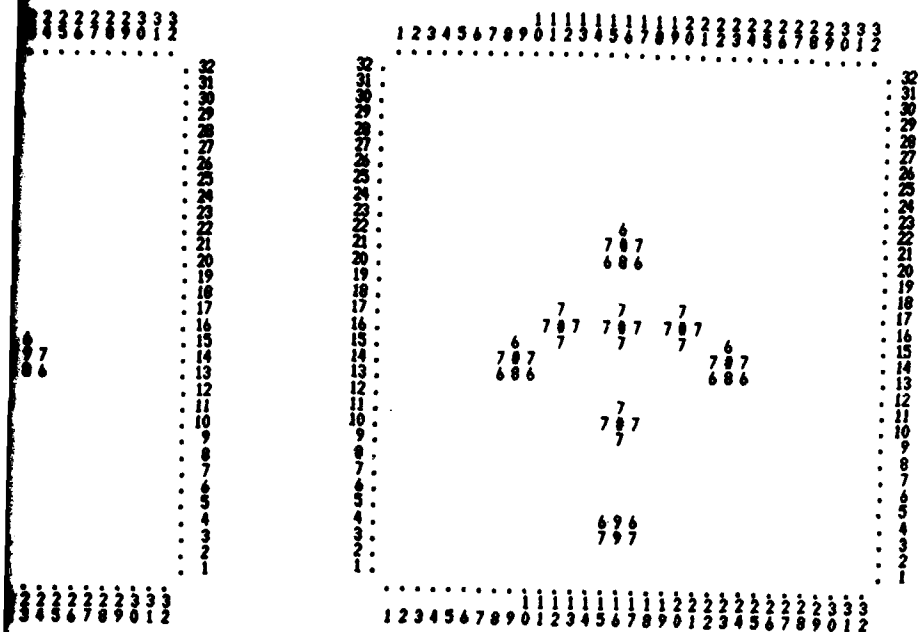

C. $\theta_0 = 90°$

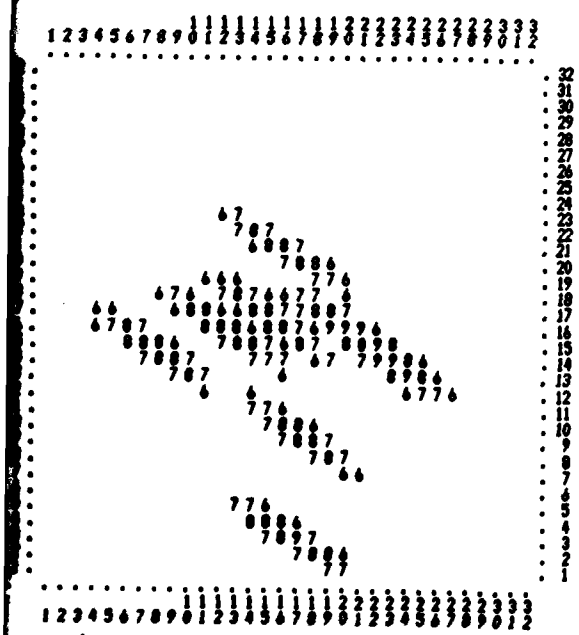

E. $\theta_0 = 150°$

Figure 3. Simulated Aircraft Image--Curl Processing Bandwidth Factor = 2

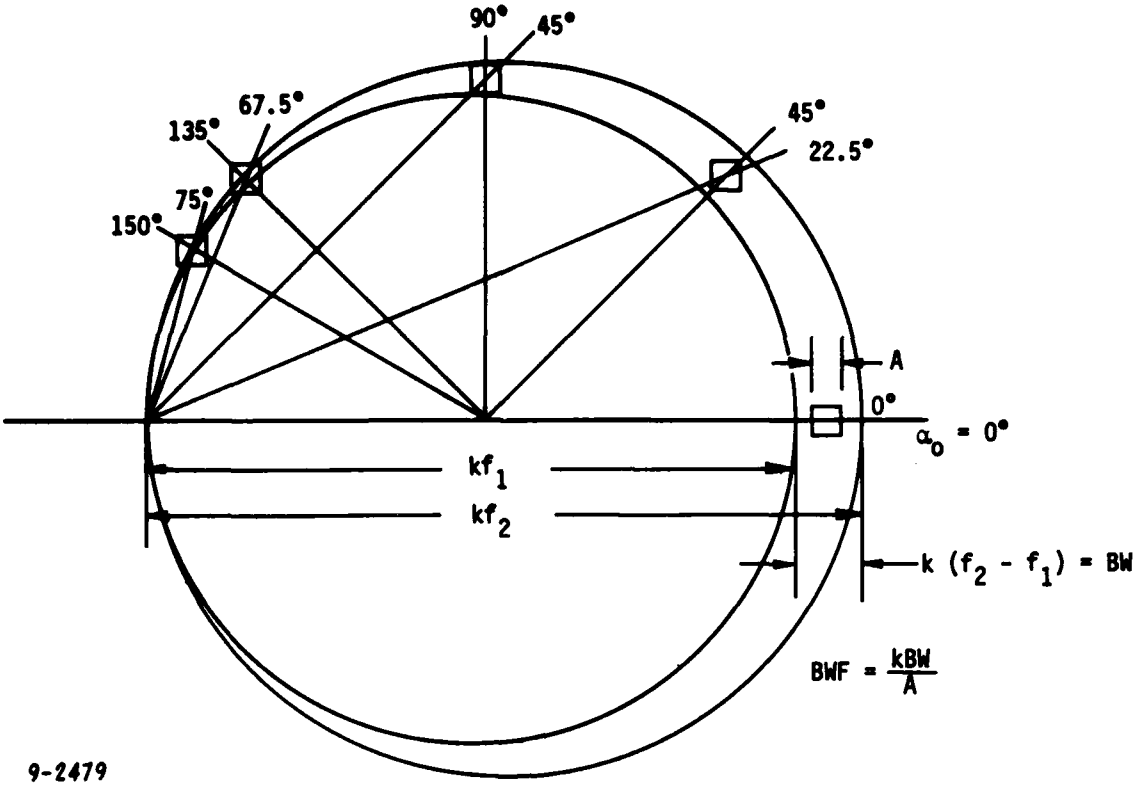

Figure 4. Curl Data Storage With Fixed Aperture Size and Orientation (For $\alpha_o = 0^o$ and BWF = 2)

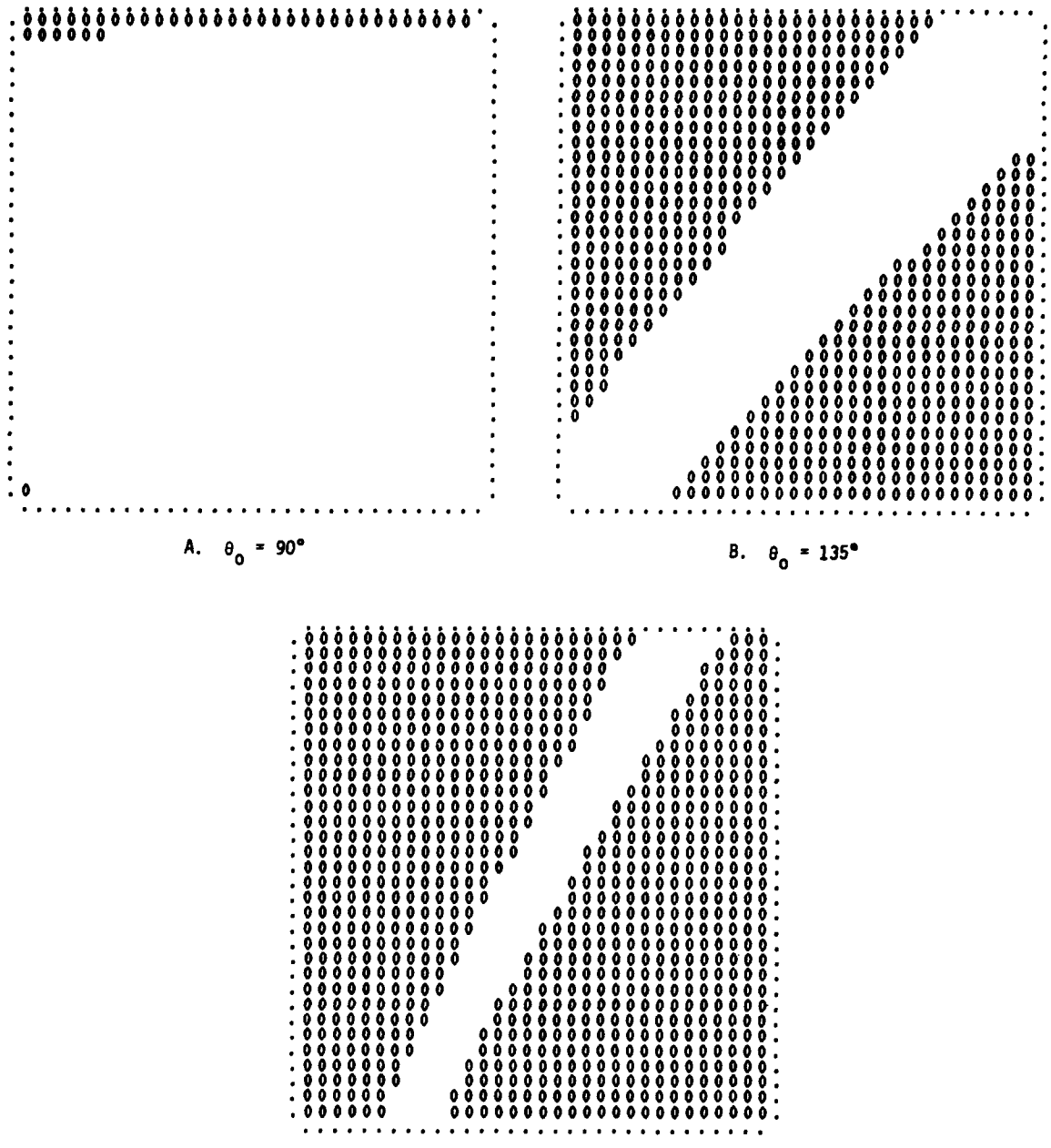

Figure 5. Data Aperture Showing Data Exclusion (For $\alpha_o = 0^o$ and BWF = 2)

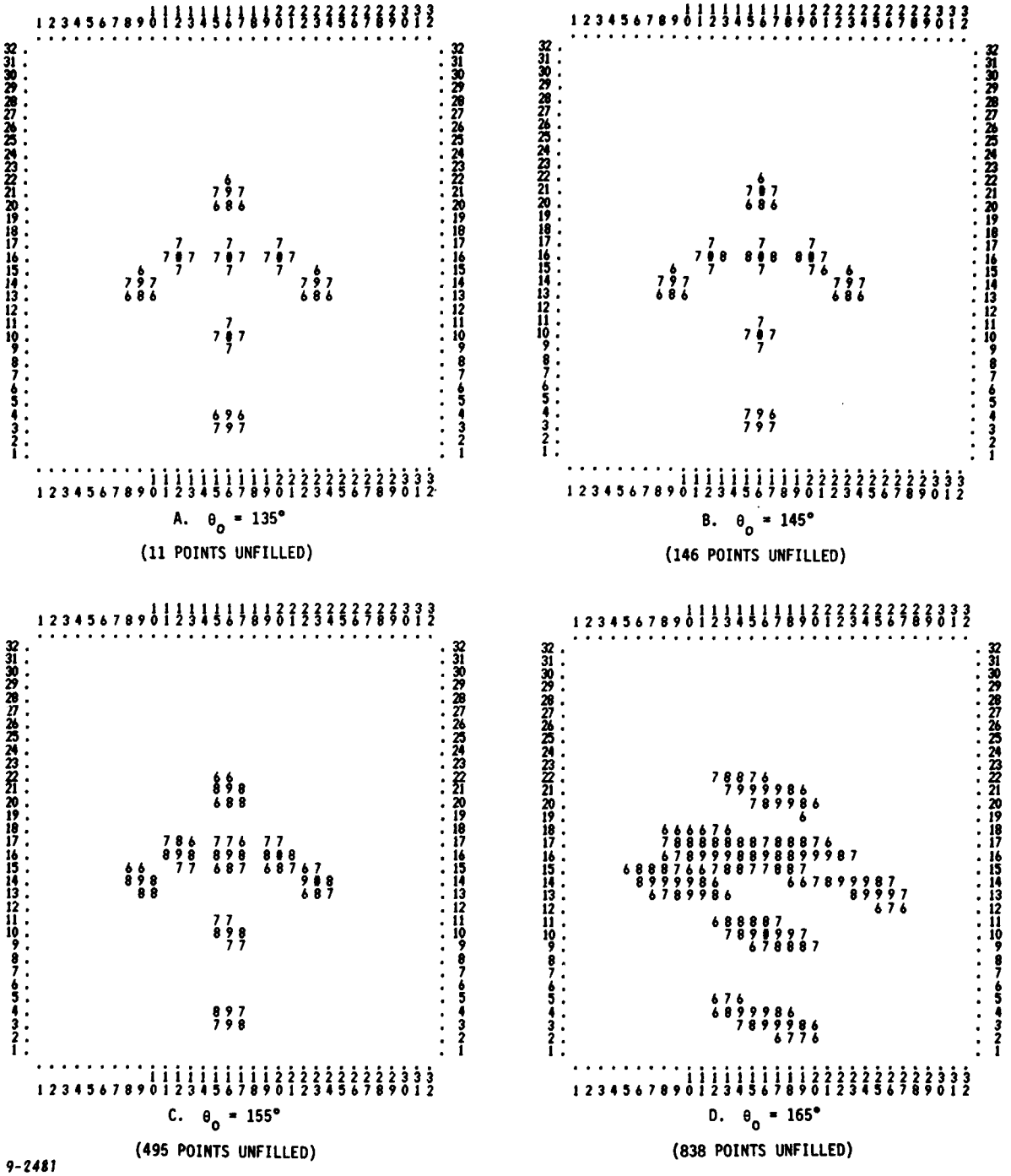

Figure 6. Simulated Aircraft Image--Curl Processing--Bandwidth Factor = 10

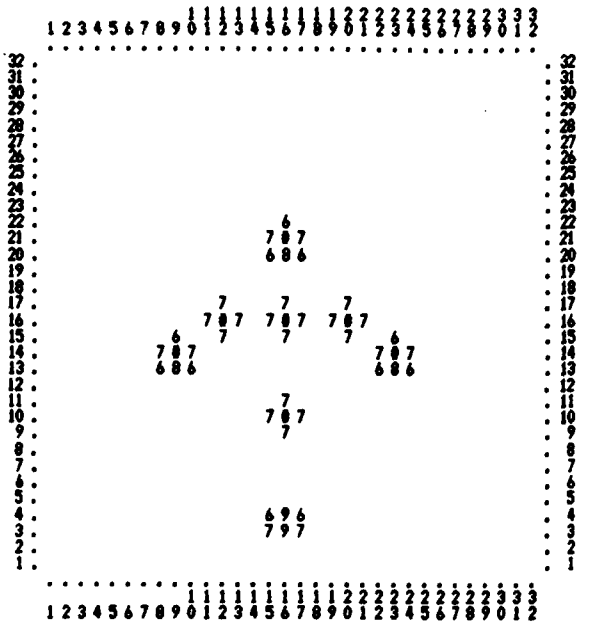

A. $\theta_0 = 0°$

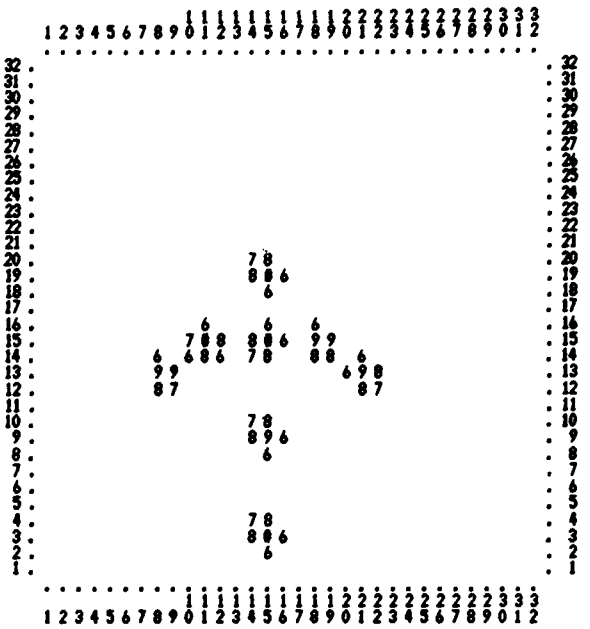

B. $\theta_0 = 45°$

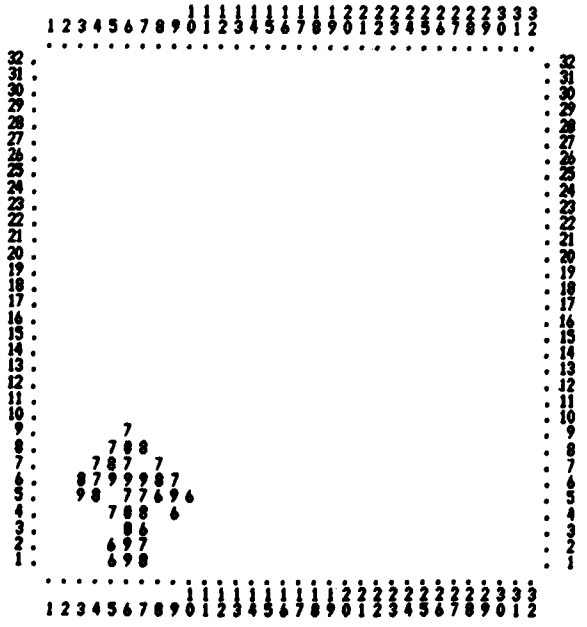

D. $\theta_0 = 135°$

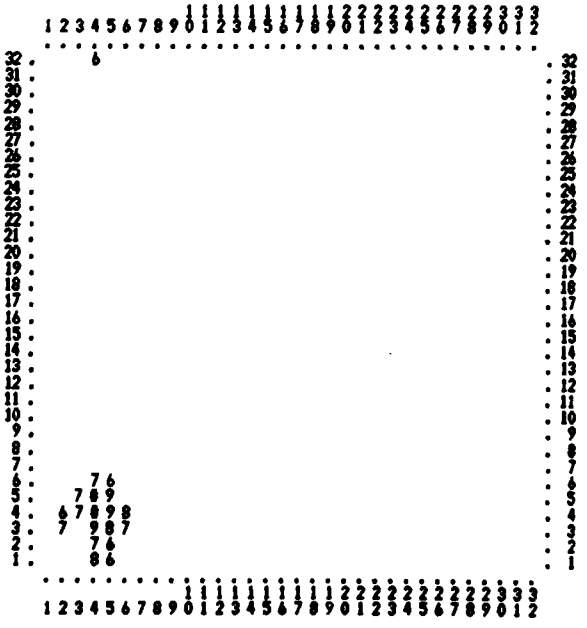

E. $\theta_0 = 150°$

9-2482

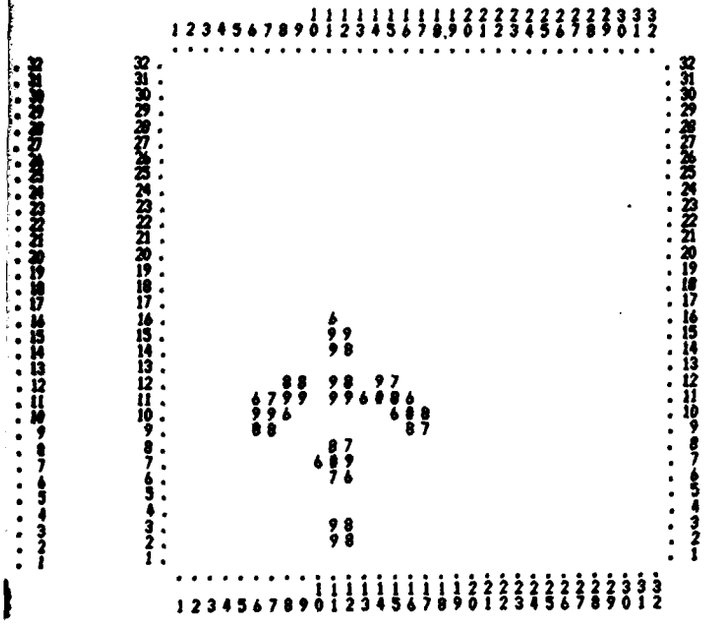

C. $\theta_0 = 90°$

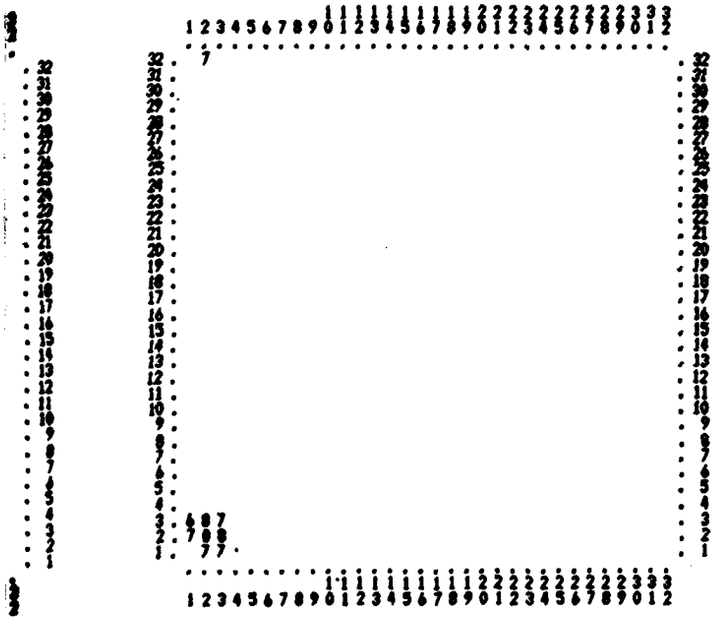

F. $\theta_0 = 165°$

Figure 7. Simulated Aircraft Image--Rotating Target--Bistatic Polar Processing

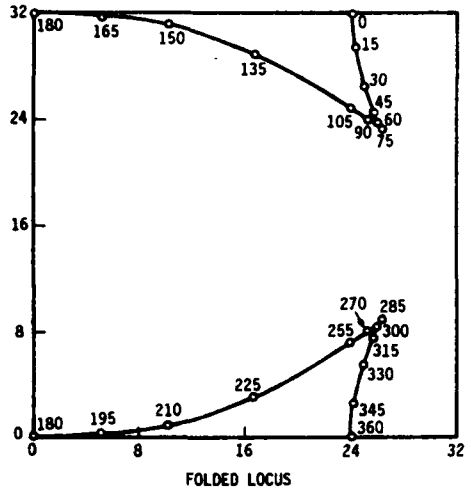

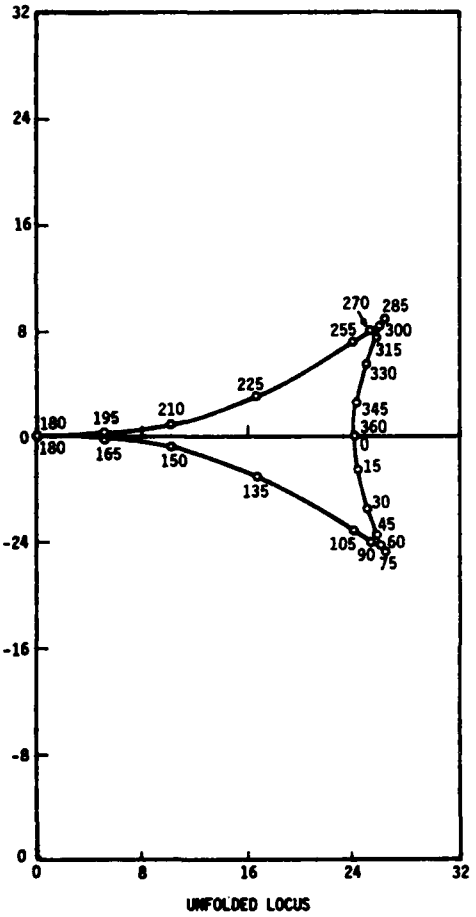

A. TARGET POINT LOCUS - POLAR PROCESSING
X = 24 Y = 0 α_0 = 0°

9-2483

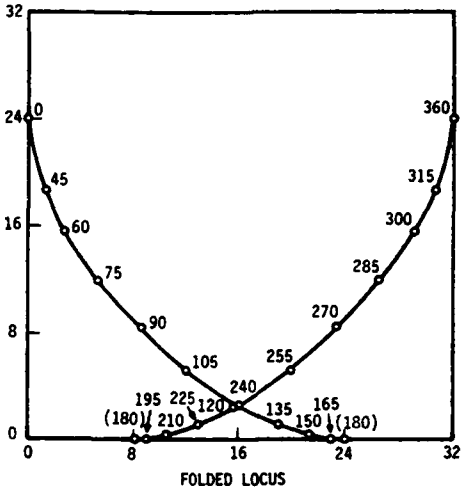

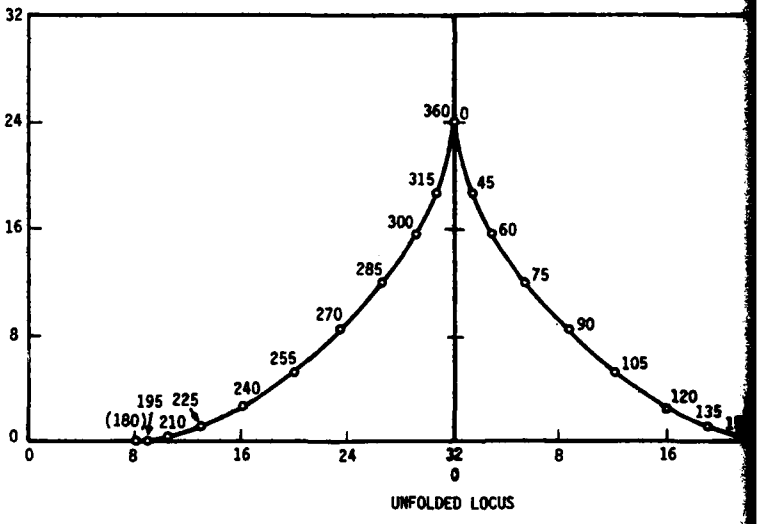

B. TARGET POINT LOCUS - POLAR PROCESSING
X = 0 Y = 24 α_0 = 0°

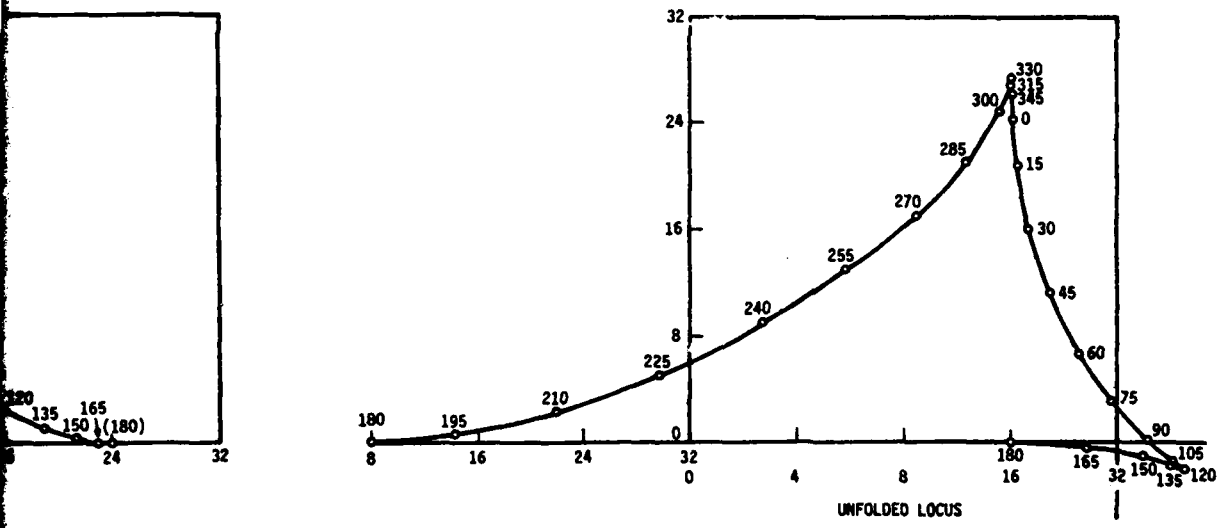

Figure 8. Locus of Single Target Points--Bistatic Polar Processing

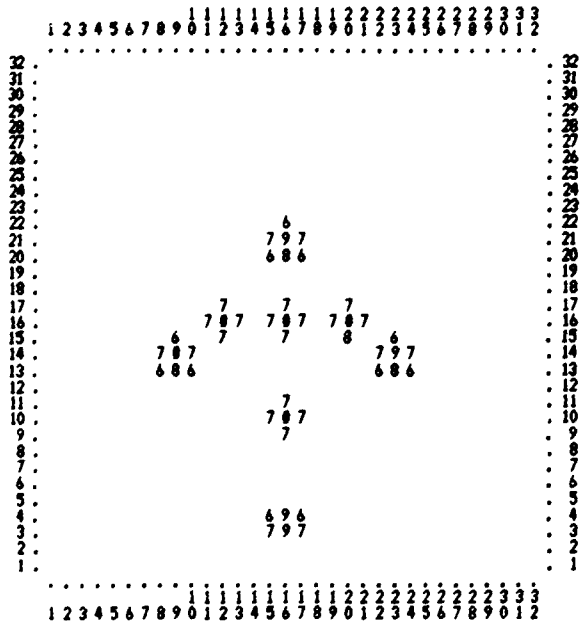

A. θ_0 = 0°; X, Y OFFSET = 0, 0

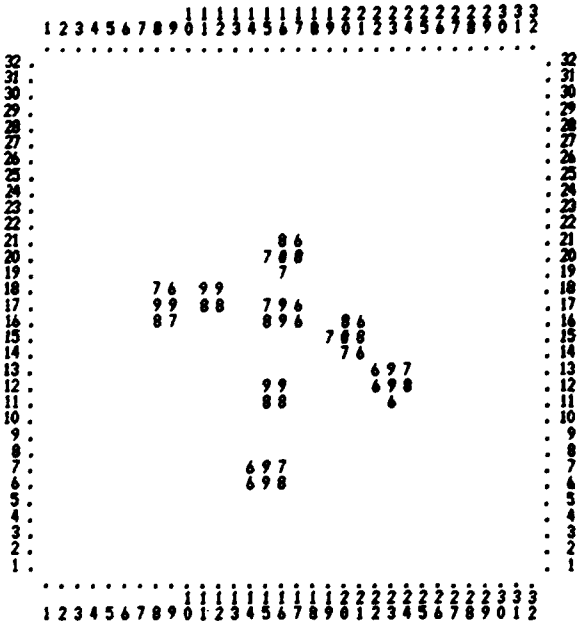

B. θ_0 = 45°; X, Y OFFSET = -2, 9

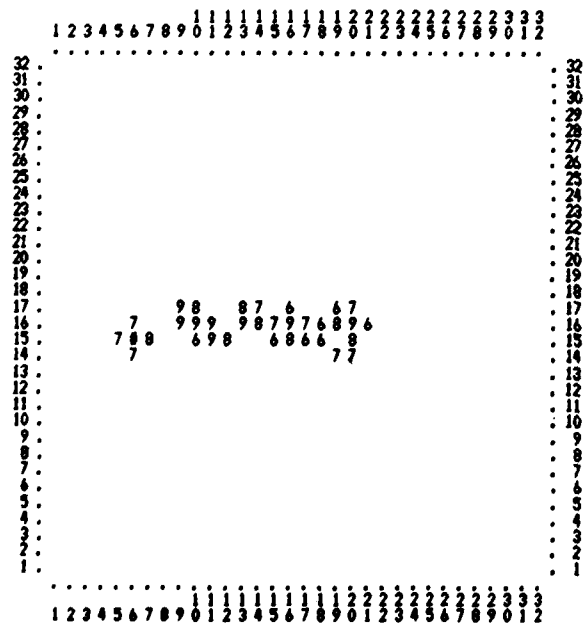

D. θ_0 = 135°; X, Y OFFSET = -8, -15

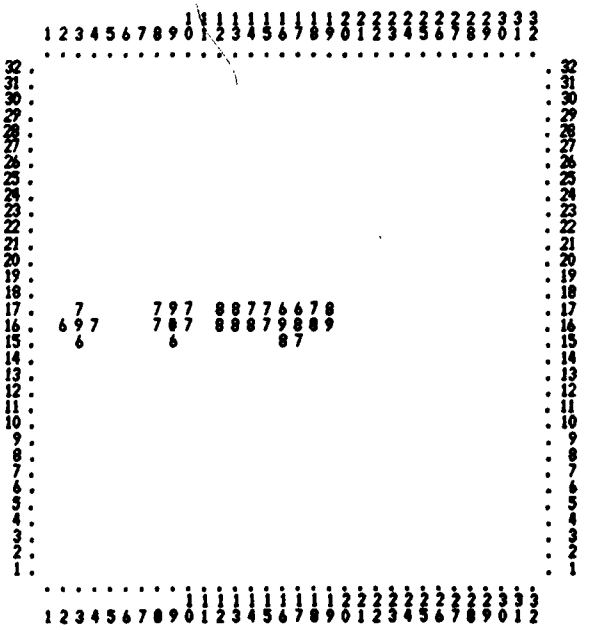

E. θ_0 = 150°; X, Y OFFSET = -8, -15

9-2484

Fig

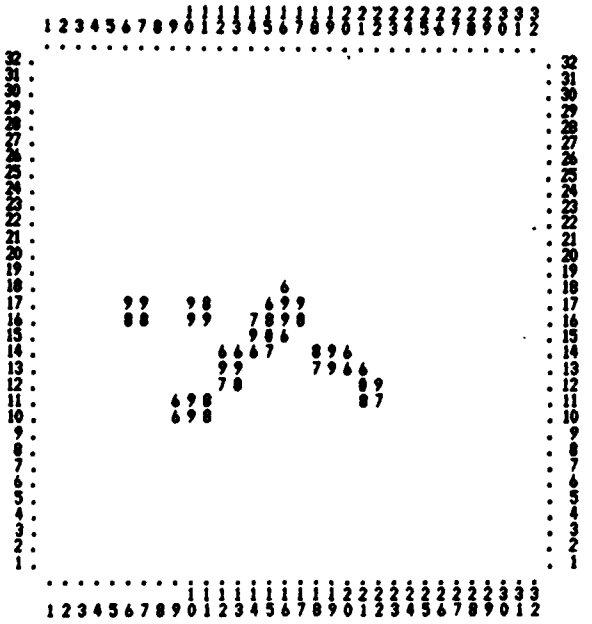

C. θ_0 = 90°; X, Y OFFSET = -8, 15

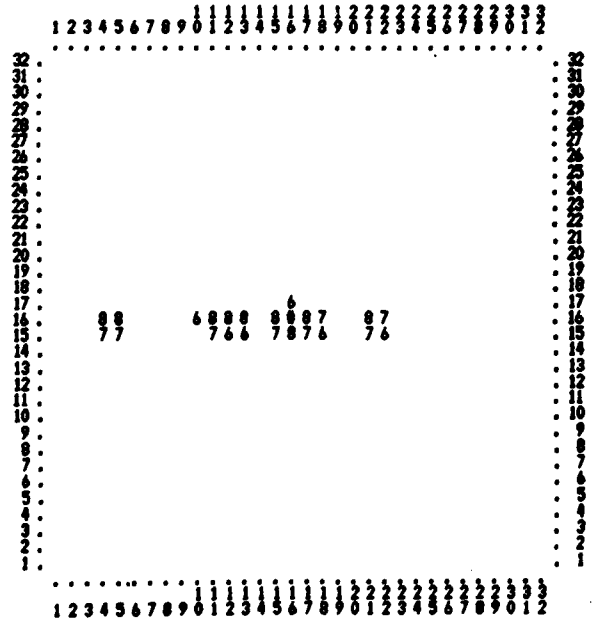

F. θ_0 = 165°; X, Y OFFSET = -3, -16

Figure 9. Simulated Aircraft Image--General Case--Bistatic Polar Processing

3. BISTATIC IMAGING IN THREE-DIMENSIONAL RADAR SPACE

Two-dimensional image processing of the two-dimensional bistatic SAR geometry case is extended in this section to the three-dimensional bistatic SAR geometry case. For two-dimensional processing, it is necessary to determine the performance limitations due to the radar or target third dimension. The primary effect of the radar third dimension is in determining the orientation of the "image projection-plane." For radar imaging of aircraft from the ground, the target is nearly planar, and the radar designer is primarily concerned with the orientation and scale of the image relative to the target; that is, is the image a plan view, side view, or front view of the aircraft target? The projection plane is determined by a combination of the orientation of the target relative to a reference plane (containing the target center, transmitter and receiver), and the orientation of the projection plane relative to the reference plane, determined by the target (or radar) velocity component normal to the reference plane. This target perspective investigation is the primary subject of the remainder of this report; tradeoff curves are presented to allow convenient evaluation of the effect of various parameters upon perspective.

If the target is not planar, or if the target plane is not closely parallel with the image projection plane, then slight changes in the image plane or target orientation occurring over the interval of data collection (the synthetic aperture) will cause loss (or limitation) of resolution. The resolution loss increases as: the target "height" increases, the target orientation change increases, or the image plane orientation change increases. This effect is explored in the Appendix for the simple case of a target undergoing rotation only. The rotating target case is shown to be highly similar to that for monostatic radar, allowing easy extrapolation to the bistatic radar case.

In the following two sections, the bistatic Doppler gradient vector (subsection 3.1) and the bistatic image projection direction (subsection 3.2) are defined. A derivation of the bistatic Doppler gradient vector and bistatic image projection direction can be found in the Appendix. In subsection 3.3, the orientation of the image projection plane in terms of elevation angle is defined. Subsection 3.4 presents design tradeoff curves of elevation angle versus three-dimensional bistatic geometry.

3.1 DEFINITION OF THE BISTATIC DOPPLER GRADIENT VECTOR

The bistatic Doppler gradient vector, $\frac{\nabla(\lambda \omega_D)}{2\pi}$ is determined by the vector sum of of the receiver Doppler gradient vector $\nabla(\vec{\omega}_R \times \hat{R})$ and the transmitter Doppler gradient vector, $\nabla(\vec{\omega}_X \times \hat{X})$.* The $\nabla(\vec{\omega}_R \times \hat{R})$ vector is determined by using the plane containing the receiver field-of-view (FOV) center and relative velocity vector between the FOV center and receiver; it is identical to the Doppler gradient vector of a monostatic SAR at the receiver position. The transmitter Doppler gradient vector is determined in the same way by considering a monostatic SAR at the transmitter location. A derivation of the bistatic Doppler gradient vector is given in the Appendix.

---

*$\vec{\omega}_R$ (Ω_X) = receiver (transmitter) rotation rate

$\hat{R}$ ($\hat{X}$) = receiver (transmitter) unit vector direction

3.2 BISTATIC IMAGE PROJECTION DIRECTION

If, for the bistatic three-dimensional geometry case, the usual assumption is made that the target ranges to the receiver and transmitter are large, then:

- Iso-range contours are planes orthogonal to the bistatic angle bisector direction
- Iso-Doppler contours are planes orthogonal to the bistatic Doppler gradient vector

The iso-range and iso-Doppler contours intersect in straight, parallel lines. Any point on a given intersection line is at the same range and Doppler as any other point on the same intersection line. Then, all points on a given intersection line will image into a single point. The intersection lines then give the image projection direction which is unique in a given geometry. Any plane orthogonal to the projection direction is definable as an image projection plane and the projection direction is then the normal to the image projection plane.

It is important to note that the iso-range contours (planes) are not orthogonal to the iso-Doppler contours (planes) unless the bistatic angle is zero (monostatic case).

The following equations (derived in the Appendix) give the direction of the image projection plane normal, $\vec{N}$, for the indicated SAR geometries:

- Monostatic (General Target Motion)

$$\vec{N} = \vec{M} \times \vec{\Omega}_T \times \vec{M} \tag{1}$$

- Bistatic (Rotating Target)

$$\vec{N} = \vec{B} \times \vec{\Omega}_T \times \vec{B} \tag{2}$$

- Bistatic (Translating Target)

$$\vec{N} = (1 + \cos\beta)\,(\vec{\Omega}_R + \vec{\Omega}_X) - (\hat{X} \cdot \vec{\Omega}_R)\,\hat{R} - (\hat{R} \cdot \vec{\Omega}_X)\,\hat{X} \tag{3}$$

- Bistatic (Translation and Rotation)

$$\vec{N} = (1 + \cos\beta)\,(\vec{\Omega}_R + \vec{\Omega}_X) - (\vec{\Omega}_R \cdot \vec{B})\,\hat{R} - (\vec{\Omega}_X \cdot \vec{B})\,\hat{X} \tag{4}$$

where,

β = bistatic angle

$\vec{M}$ = monostatic SAR position vector with respect to target (called $2\vec{X}$ in Appendix A)

$\vec{B}$ = bistatic angle bisector direction

$\vec{\Omega}_T$ = target rotation vector

$\hat{X}$ = transmitter direction (unit vector)

$\hat{R}$ = receiver direction (unit vector)

$\vec{\Omega}_R$ ($\vec{\Omega}_X$) = bistatic rotation vector of receiver (transmitter)

Comparison of the general monostatic case (equation 1) and the bistatic case for a rotating object (equation 2) shows that the normal to the image projection plane has the same form with the monostatic radar vector $\vec{M}$ replaced by the bisector vector $\vec{B}$. For a bistatic radar configuration, with constant bistatic angle and aspect diversity generated by target rotation, a monostatic equivalent of the bistatic radar can be derived with the monostatic radar located on the bistatic angle bisector.

Comparison of the bistatic translating target case (equation 3) or the bistatic translation plus rotation case (equation 4) with the monostatic case (equation 1) shows that the image projection plane normal, $\vec{N}$, for the bistatic cases is different in form from the monostatic case. The translating (and translating plus rotating) bistatic cases cannot be simplified to a monostatic model in which the bistatic terminals are replaced by a single fixed monostatic terminal.

3.3 IMAGE PROJECTION PLANE ELEVATION ANGLE

For a translating object or bistatic SAR (refer to the Appendix), the projection plane elevation angle, θ, relative to a reference plane (containing the target FOV center, receiver and transmitter) is given by:

$$\tan\theta = \left| \frac{\vec{\Omega}_R \cdot \hat{X} - \vec{\Omega}_X \cdot \hat{R}}{\vec{\Omega}_X + (\vec{\Omega}_R) \cdot (\hat{R} \times \hat{X}) \cos \beta/2} \hat{B} \right| \tag{5}$$

where,

$\hat{X}(\hat{R})$ = transmitter (receiver) unit direction vector

$\vec{\Omega}_X(\vec{\Omega}_R)$ = transmitter (receiver) rotation vector due to target translation only

$\hat{B}$ = bistatic angle bisector unit direction vector

β = bistatic angle

This expression allows the magnitude and direction of θ to be easily separated with:

- direction $= \hat{B}$
- magnitude $= \theta = \tan^{-1}\left[\dfrac{\vec{\Omega}_R \cdot \hat{X} - \vec{\Omega}_X \cdot \hat{R}}{(\vec{\Omega}_X + \vec{\Omega}_R) \cdot (\hat{R} \times \hat{X}) \cos \beta/2}\right]$ (6)

The magnitude of θ is a good measure of the three-dimensionality of a bistatic engagement and is presented in a set of tradeoff curves in subsection 3.4. The translating target case (no target rotation) is of particular interest as applicable to imaging a nonmaneuvering aircraft with a ground-based bistatic SAR.

3.4 DESIGN TRADEOFF FOR A SPECIFIC ENGAGEMENT GEOMETRY

The specific engagement geometry for imaging a noncooperative aircraft with a ground-based bistatic synthetic aperture radar will now be considered and analyzed. Geometric image distortion will be considered in terms of the average elevation (tilt) angle of the image projection plane for the synthetic aperture. The derivation of the image projection plane elevation angle given in this section is equivalent to that given in subsection 3.3, but lends more readily to a series of pictorials to give insight and understanding to the derivation.

The remainder of this section develops tradeoff curves to assist the system designer in placement of transmitter(s) and receiver(s) to minimize image distortion. Additionally, the tradeoff curves can be used in an operational multistatic system to choose the optimum transmitter and receiver to minimize image distortion.

3.4.1 Coordinate System

Consider a ground-based bistatic SAR with the transmitter and receiver arbitrarily located with respect to a FOV containing an aircraft to be imaged in flight. Without loss in generality, the coordinate system can be oriented so that the receiver, transmitter, and FOV center fall in the X-Y plane. In addition, the transmitter can be placed along the X-axis and the target FOV center at the origin. The target aircraft velocity vector is then generally not in the X-Y plane and can have a significant component of velocity in the Z-axis direction.

Figure 10 gives the relative positions and directions of the receiver, transmitter, FOV center, and the target velocity vector in this coordinate system. Also indicated on the figure is the bistatic angle, β, and the direction of the bistatic angle bisector (which also falls in the X-Y plane). A general rule of thumb for small bistatic angles is that, to form a synthetic aperture for a given engagement and image resolution, the direction of the angle bisector must change direction by a minimum prescribed angular amount with respect to the target. If Figure 10 is valid at the arithmetic average position of the bisector, it is also valid at the angular center of the synthetic aperture. Further, if the coordinate system origin is fixed to the target FOV center in time, the transmitter and receiver will have identical velocity vectors equal to the target velocity vector. The transmitter and receiver will then be in the X-Y plane only at the center of the synthetic aperture (unless the Z-component of velocity is zero, in which case the transmitter, receiver, and FOV center are always coplanar). The X-Y plane will hereafter be called the fiducial plane.

3.4.2 Image Projection Plane Derivation

The orientation of the image projection plane at a given instant of time is determined by the bistatic angle bisector direction at that instant of time and by the resultant transmitter/receiver Doppler gradient vector at that instant of time. The resultant bistatic Doppler gradient vector is the vector sum of the transmitter and receiver Doppler gradient vectors.

3.4.2.1 Resultant Doppler Gradient Vector-The receiver Doppler gradient vector can be computed as if the receiver were a monostatic SAR. The direction of the receiver Doppler gradient vector is then simply given by the tangential component of velocity to the receiver/target direction in the plane formed by the receiver position and the target velocity vector. The plane formed by the receiver position and the target velocity vector is the image projection plane for a monostatic SAR at the receiver location (hereafter called the receiver monostatic image plane).

The transmitter Doppler gradient vector can be found in the same way by considering a monostatic SAR at the transmitter location and computing the tangential component of target velocity in the transmitter monostatic image projection plane.

The receiver monostatic Doppler gradient vector is formed by taking the tangential component of target velocity in the receiver image projection plane and normalizing by the receiver to target distance. The transmitter Doppler gradient vector is computed in an identical fashion considering the transmitter as a monostatic SAR. The resultant bistatic Doppler gradient vector is the vector sum of the transmitter rotational vector and the receiver rotational vector.

Figure 11 considers the transmitter position, target position, and target velocity vector at the center of the synthetic aperture. The transmitter monostatic image plane is determined by $\vec{V}$ and $\vec{X}$ and is indicated on the figure by plane ABCO. The locus of all points perpendicular to the transmitter direction at the origin of the coordinate system is given by plane DCEO which in this case happens to be the Y-Z plane. The tangential component of target velocity $\vec{V}_{TX}$, in the transmitter monostatic image projection plane is the projection of $\vec{V}$ on the intersection of planes ABCO and DCEO. The transmitter Doppler gradient vector is then formed by normalizing $\vec{V}_{TX}$ by the magnetude of $\vec{X}$ to get $\vec{\omega}_{TX}$,* as indicated on the figure. It is important to note that Figure 11 is not drawn to scale with respect to the relative lengths of the vectors $\vec{V}$ and $\vec{X}$ for clarity of demonstration.

Figure 12 considers the receiver position, target position, and target velocity vector at the center of the synthetic aperture. The receiver monostatic image plane is determined by $\vec{V}$ and $\vec{R}$ and is indicated on the figure by plane ABCO. The locus of all points perpendicular to the receiver direction (which is in the X-Y plane) at the origin of the coordinate system is given by plane DAEO. The construction line $R_{\perp}$, which is perpendicular to the receiver direction in the X-Y plane, has been added to clarify the picture. The tangential component of the target velocity, $\vec{V}_{TR}$, in the receiver monostatic image projection plane is the projection of $\vec{V}$ on the intersection of planes ABCO and DAEO. The receiver Doppler gradient vector is then formed by normalizing $\vec{V}_{TR}$ by the magnitude of $\vec{R}$ to get $\vec{\omega}_{TR}$ as indicated on the figure. Again, it is important to note that Figure 12 is not drawn to scale with respect to the relative lengths of the vectors $\vec{V}$ and $\vec{R}$ for clarity of demonstration.

---

*In Appendix A $\vec{\Omega}^T$ is used instead of $\vec{\omega}_T$

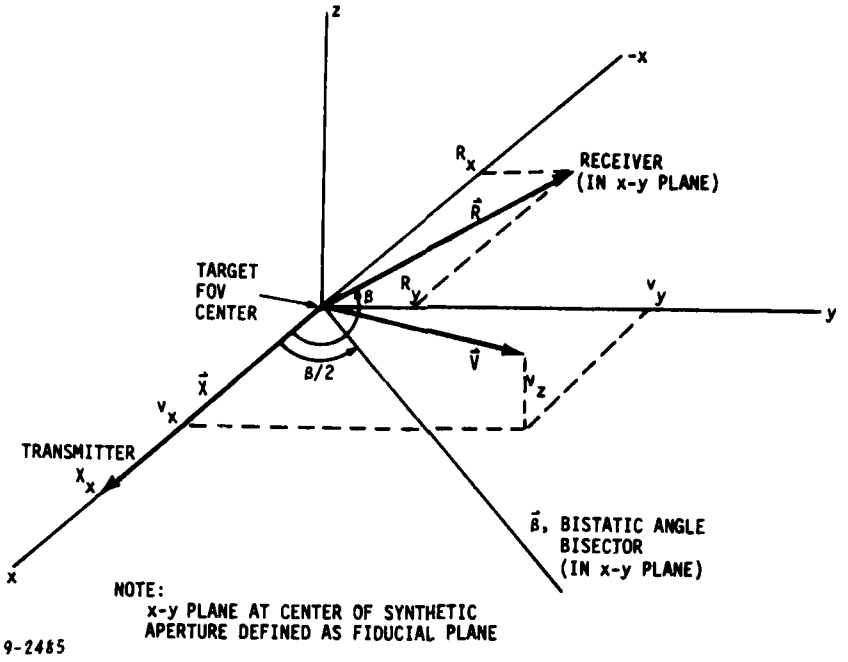

Figure 10. Geometry at Center of Synthetic Aperture

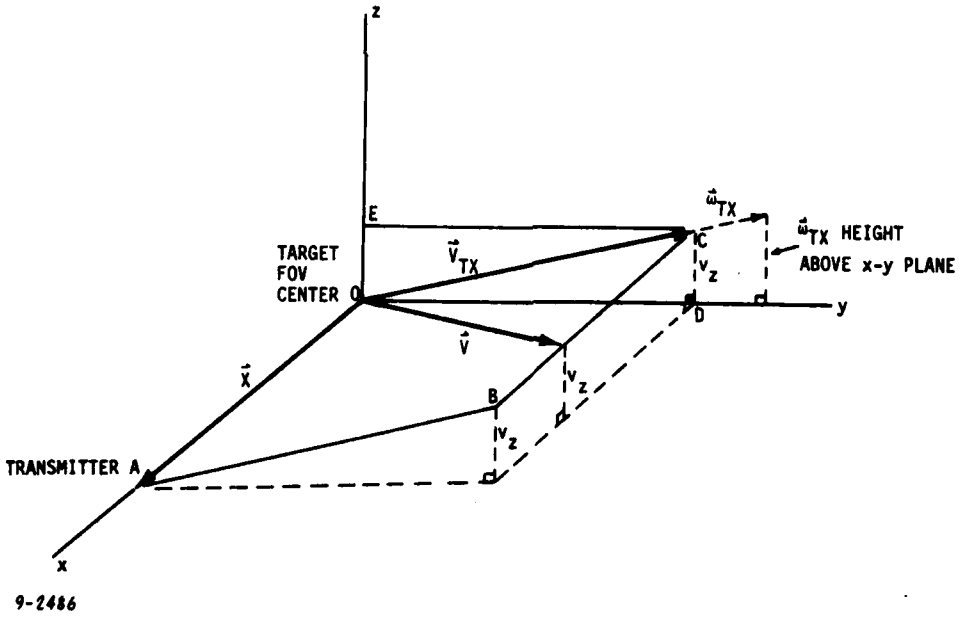

Figure 11. Construction of $\vec{\omega}_{TX}$ Vector

Using Figures 11 and 12, the transmitter and receiver Doppler gradient vectors, $\vec{\omega}_{TX}$ and $\vec{\omega}_{TR}$, are determined at the center of the synthetic aperture to be:

$$\vec{\omega}_{TX} = \left(0, \frac{v_y}{|\vec{X}|}, \frac{v_z}{|\vec{X}|}\right) \tag{7}$$

$$\vec{\omega}_{TR} = \left(\frac{R_y [R_y v_x - R_x v_y]}{|\vec{R}|^3}, \frac{R_x [R_x v_y - R_y v_x]}{|\vec{R}|^3}, \frac{v_z}{|\vec{R}|}\right) \tag{8}$$

where,

$(X_x, 0, 0)$ = transmitter position

$(R_x, R_y, 0)$ = receiver position

$(0, 0, 0)$ = target FOV center

(v_x, v_y, v_z) = target velocity

$|\vec{X}|$ = magnitude of the transmitter direction vector

$|\vec{R}|$ = magnitude of the receiver direction vector

The bistatic resultant Doppler gradient vector, $\vec{\omega}$, is given by:

$$\vec{\omega} = \vec{\omega}_{TX} + \vec{\omega}_{TR} \tag{9}$$

Figure 13 gives the vector sum of $\vec{\omega}_{TR}$ and $\vec{\omega}_{TX}$. The z-component, ω_z, of $\vec{\omega}$ will be of interest later and is indicated on the figure.

3.4.2.2 Bistatic Angle Bisector Direction-The bistatic angle bisector direction at the center of the synthetic aperture can be determined from Figure 10 to be given by:

$$\vec{B} = (\cos [\beta/2], \sin [\beta/2], 0) \tag{10}$$

where β = bistatic angle formed by the transmitter, target FOV center and the receiver. $\vec{B}$ is in the X-Y plane at the center of the synthetic aperture.

3.4.2.3 Image Projection Plane Elevation Angle-The image projection plane elevation angle with respect to the fiducial plane at the center of the synthetic aperture is determined from Figure 14. From the figure, the resultant Doppler gradient vector, $\vec{\omega}$, is obtained from Figure 1 along with its z-component, ω_z. The bisector direction vector, $\vec{B}$, is obtained from Figure 1. The bistatic image projection plane is then determined by the directions of $\vec{\omega}$ and $\vec{B}$, and is indicated in Figure 14 by plane ABCO.

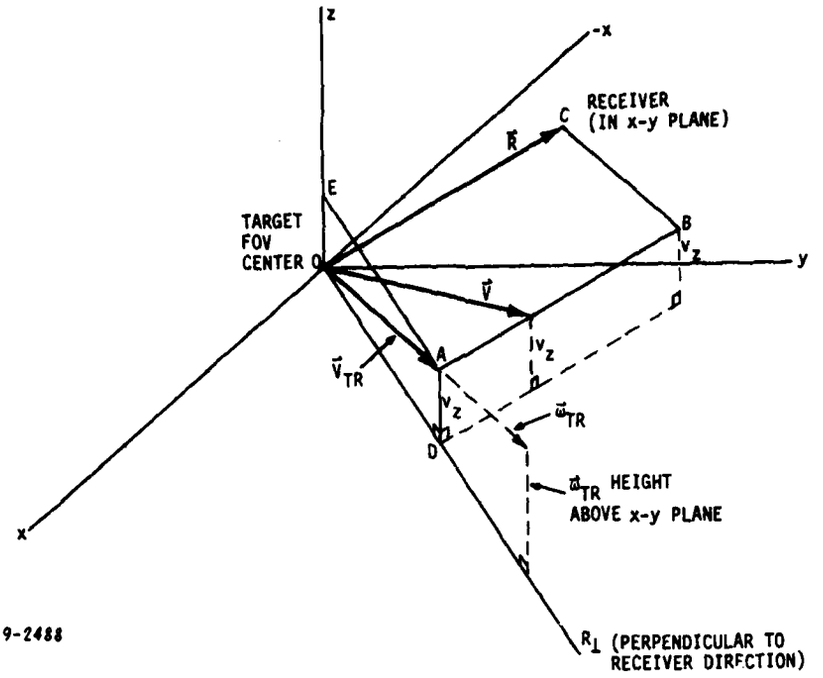

Figure 12. Construction of $\vec{\omega}_{TR}$ Vector

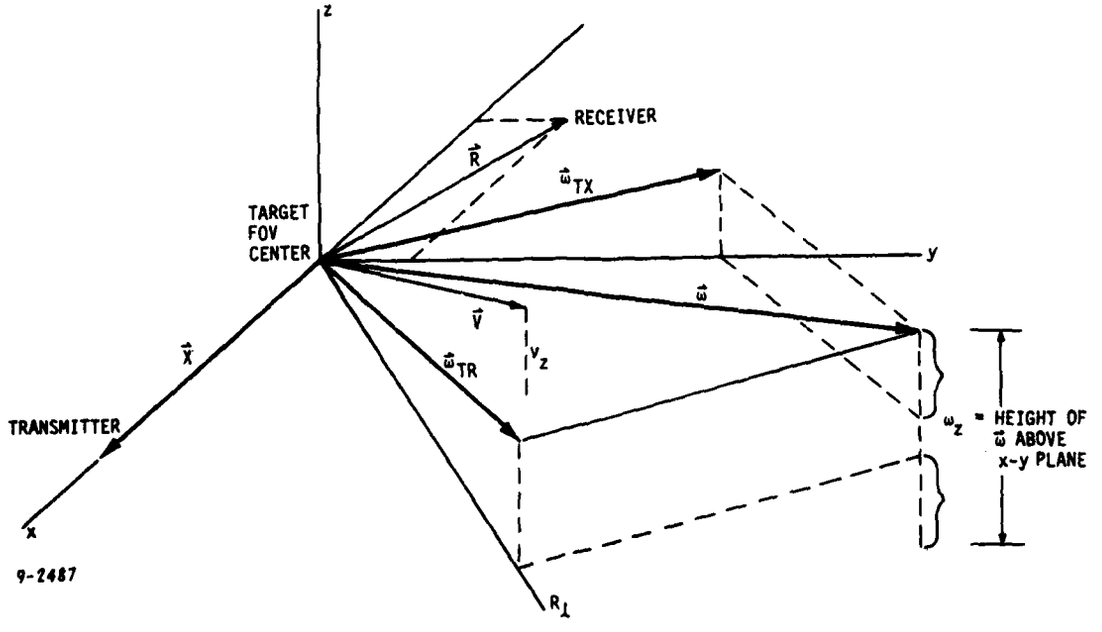

Figure 13. Construction of $\vec{\omega}$ Vector

From Figure 14, $\vec{D}$ is in the image projection plane and gives the distance $\vec{\omega}$ is from $\vec{B}$. The vector $\vec{A}$ is in the fiducial plane and connects the intersection of ω_z with the intersection of $\vec{D}$ and $\vec{B}$. Then the elevation angle of the image projection plane, θ, as indicated on the figure, is given by:

$$\theta = \tan^{-1}\left[\frac{\omega_z}{|\vec{A}|}\right]$$

or using equations 7 through 10:

$$\theta = \tan^{-1}\left[\frac{v_z\,[|\vec{X}| + |\vec{R}|]}{\cos(\beta/2)\,[|\vec{X}|\,(v_x \sin\beta - v_y \cos\beta) - |\vec{R}|\,v_y]}\right]^{*} \tag{11}$$

where,

(v_x, v_y, v_z) = target velocity vector

β = bistatic angle

$|\vec{X}|$ = distance transmitter is from origin (target FOV center)

$|\vec{R}|$ = distance receiver is from origin (target FOV center)

Rearranging terms in equation 11 gives:

$$\theta = \tan^{-1}\left[\frac{1}{\cos(\beta/2)\left[\frac{|\vec{X}|}{|\vec{X}| + |\vec{R}|}\left(\frac{v_x}{v_z}\sin\beta - \frac{v_y}{v_z}\cos\beta\right) - \frac{|\vec{R}|}{|\vec{X}| + |\vec{R}|}\frac{v_y}{v_z}\right]}\right] \tag{12}$$

Let,

$$\frac{|\vec{R}|}{|\vec{X}| + |\vec{R}|} = \underline{R}, \text{ then } \frac{|\vec{X}|}{|\vec{X}| + |\vec{R}|} = 1-\underline{R} \text{ for } 0 \le \underline{R} \le 1,$$

and equation 12 can be rewritten as:

$$\theta = \tan^{-1}\left[\frac{1}{\cos(\beta/2)\left[(1-\underline{R})\left(\frac{v_x}{v_z}\sin\beta - \frac{v_y}{v_z}\cos\beta\right) - \underline{R}\frac{v_y}{v_z}\right]}\right] \tag{13}$$

*Equation 11 is shown to be identical to equation 6 (subsection 3-3) for this specific geometry in the Appendix.

The normalization by $|\vec{X}| + |\vec{R}|$ has the advantage of reducing the relative distances the transmitter and receiver are from the FOV center to a single scalar $\underline{R}$ which is bounded between the finite limits of 0 and 1. $\underline{R}$ ($\underline{X}$) are measures of the bistatic imbalance of the system; that is, the difference in receiver and transmitter distances from the target.

If we let

$$\underline{v} = \sqrt{\frac{v_x^2 + v_y^2}{v_z}}$$

and

$$\Phi = \tan^{-1}\left[\frac{v_y}{v_x}\right]$$

then

$$\frac{v_x}{v_z} = \underline{v}\cos\Phi \text{ and } \frac{v_y}{v_z} = \underline{v}\sin\Phi$$

and equation 13 can be rewritten as:

$$\theta = \tan^{-1}\left[\frac{1}{\underline{v}\cos(\beta/2)\left[\sin(\beta-\Phi) - \underline{R}\left|\sin(\beta-\Phi) + \sin\Phi\right|\right]}\right] \qquad (14)$$

which is the elevation angle, θ, of the image projection plane with respect to the fiducial plane.

From equation 14 and referencing Figure 15, $\underline{v}$ is the ratio of the target velocity component in the fiducial plane to the component of velocity perpendicular to the fiducial plane and is a measure of the degree of deviation from the two-dimensional geometry case. As $\underline{v}$ becomes large, $\sqrt{v_x^2 + v_y^2}$ becomes more significant than v_z and the geometry approaches two-dimensional. As $\underline{v}$ becomes small, v_z dominates and the geometry is highly three-dimensional.

From Figure 15 and equation 14, the angle Φ describes the direction of the target velocity vector projection on the fiducial plane with respect to the transmitter direction. It is important to note that the expression for θ could be renormalized so that Φ is referenced to either the receiver direction or the bistatic angle bisector direction.

Before presenting tradeoff plots for receiver, transmitter, and target geometries, a few general comments are in order.

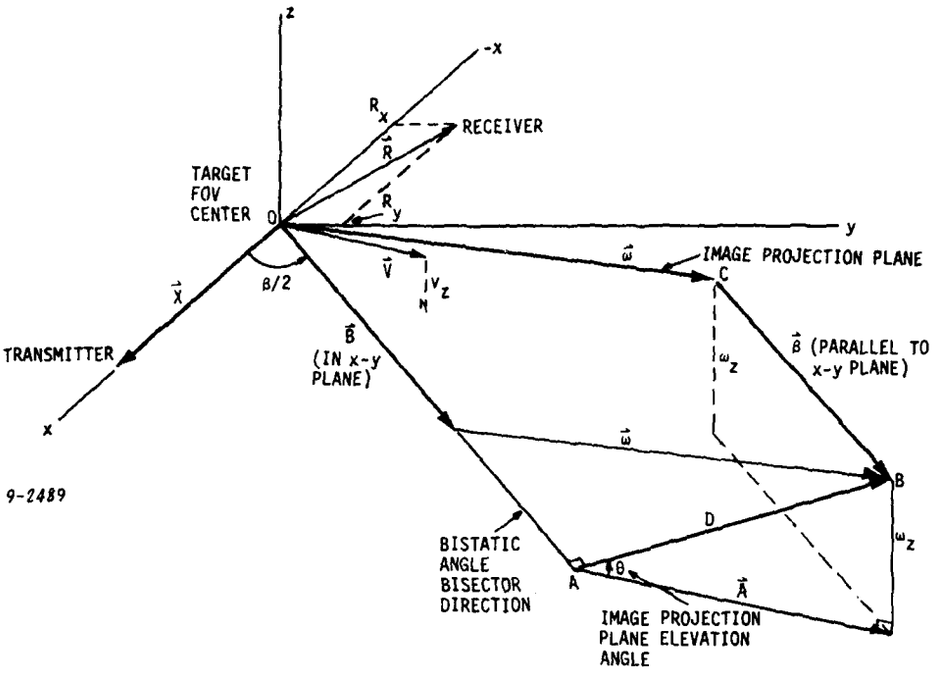

Figure 14. Construction of Image Projection Plane and Elevation Angle

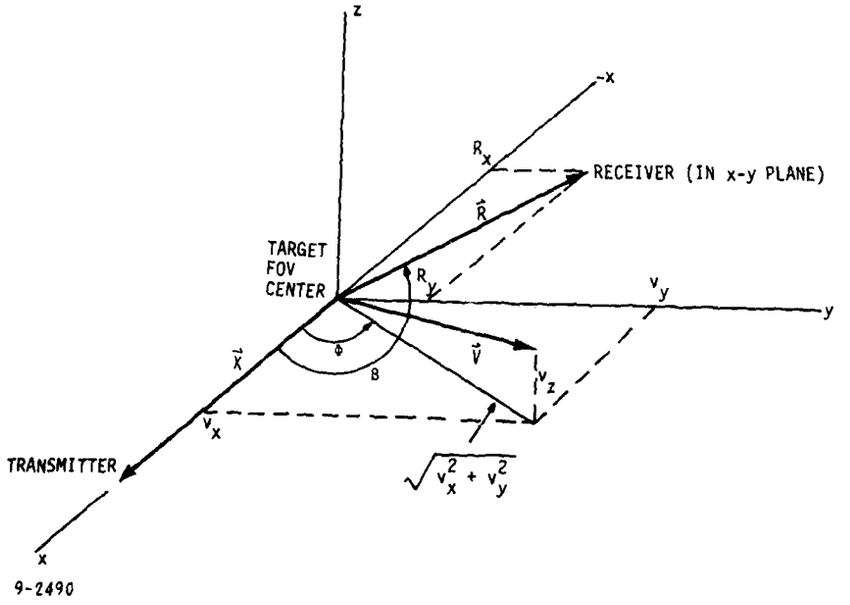

Figure 15. Geometric Parameter Normalization

The image projection plane elevation angle and the azimuth angle are of significance in relationship to scatterers on the target. For example, consider an aircraft flying straight and level at an altitude that is of the same magnitude as the distance to the transmitter or receiver. The principal scatterers of the aircraft are contained in a volume that is longer and wider than it is high. The image projection plane orientation will not be nearly parallel to the target principal scatterer plane and the image produced will not be a top (plan) view of the aircraft. This may hinder pattern matching to identify the aircraft. But, if the average orientation of the image projection plane is known, it may be possible to transform the stored pattern of the aircraft to be an equivalent view to that of the SAR image.

It is also possible that a choice of receiver sites may exist. If the orientation of the image projection plane at the center of the synthetic aperture is computed for each receiver site, then a receiver site can be chosen that minimizes the mismatch in orientation of the image projection plane with respect to the principal target scatterer plane. If the tilt angle can be minimized, then the bistatic data can be stored using two-dimensional Curl techniques with storage angles referenced to the geometry at the center of the synthetic aperture.

The expression for image projection plane elevation angle given in equation 14 is not sufficient to totally describe the orientation of the image projection plane with respect to the fiducial plane. Figure 14 shows that the azimuth angle of the image plane can be defined as the angle between the transmitter direction and the line formed by the intersection of the image plane and the fiducial plane. From the figure at the center of the synthetic aperture, the azimuth angle is one-half the bistatic angle.

It is also important to note that the elevation angle and azimuth angle of the target with respect to horizontal can easily be determined from the target altitude (from a tracking radar) and can be added vectorially to the elevation and azimuth angles of the image projection plane with respect to the fiducial plane to obtain the azimuth and elevation angles of the image plane with respect to horizontal.

3.4.3 Tradeoff Curves

Form the previous section, equation 14 can be solved for R (bistatic imbalance) to give:

$$\underline{R} = \frac{-\left[\frac{1}{\underline{v} \tan \theta \cos (\beta/2)}\right] + \sin (\beta - \Phi)}{\sin \Phi + \sin (\beta - \Phi)} \qquad (15)$$

where:

$\underline{R}$ = ratio of receiver range to sum of transmitter plus receiver ranges

$\underline{v}$ = ratio of velocity component in the fiducial plane to velocity component perpendicular to fiducial plane

Φ = angle between the transmitter direction and the velocity component in the fiducial plane

β = bistatic angle

θ = image projection plane elevation angle

For a specified maximum image projection plane elevation angle, θ_{max}, a specified $\underline{v}$ and a specified β, $\underline{R}$ can be plotted versus Φ to determine values of relative distances that the transmitter and receiver are from the target for which the image plane elevation angle will not exceed the absolute value of θ_{max}.

Figures 16 to 18 are plots of $\underline{R}$ versus Φ for the indicated values of bistatic angle, β, and velocity condition $\underline{v}$:

Figure	β (degrees)	$\underline{v}$
16A	90	5.0
16B	90	5.5
16C	90	10.0
16D	90	15.0
16E	90	18.0
16F	90	30.0
16G	90	$\rightarrow \infty$
17A	45	10.0
17B	45	15.0
18A	135	10.0
18B	135	15.0

Each figure contains plots that bound the regions of $\underline{R}$ and Φ in which θ_{max} is less than or equal to 5, 7.5, 10, and 20 degrees. A detailed discussion of the formats of the curves is in order prior to a discussion of the significance of the curves. To this end, Figure 16E will be discussed in detail.

From Figure 16E, the regions for which the conditions of θ_{max} less than or equal to 5, 7.5, 10, and 20 degrees are coded as follows:

$\theta_{max} \leq 5$ degrees	Horizontal lines
$\theta_{max} \leq 7.5$ degrees	Vertical lines
$\theta_{max} \leq 10$ degrees	Tilted lines with positive slope viewing from left to right
$\theta_{max} \leq 20$ degrees	Tilted lines with negative slope viewing from left to right

The region for which $\theta_{max} \leq 20$ degrees also includes the regions for $\theta_{max} \leq 10$, 7.5, and 5 degrees; the region for $\theta_{max} \leq 10$ degrees also includes the regions for $\theta_{max} \leq$ 7.5 and 5 degrees, and so on. The solid unhatched region is for the condition where θ_{max} > 20 degrees.

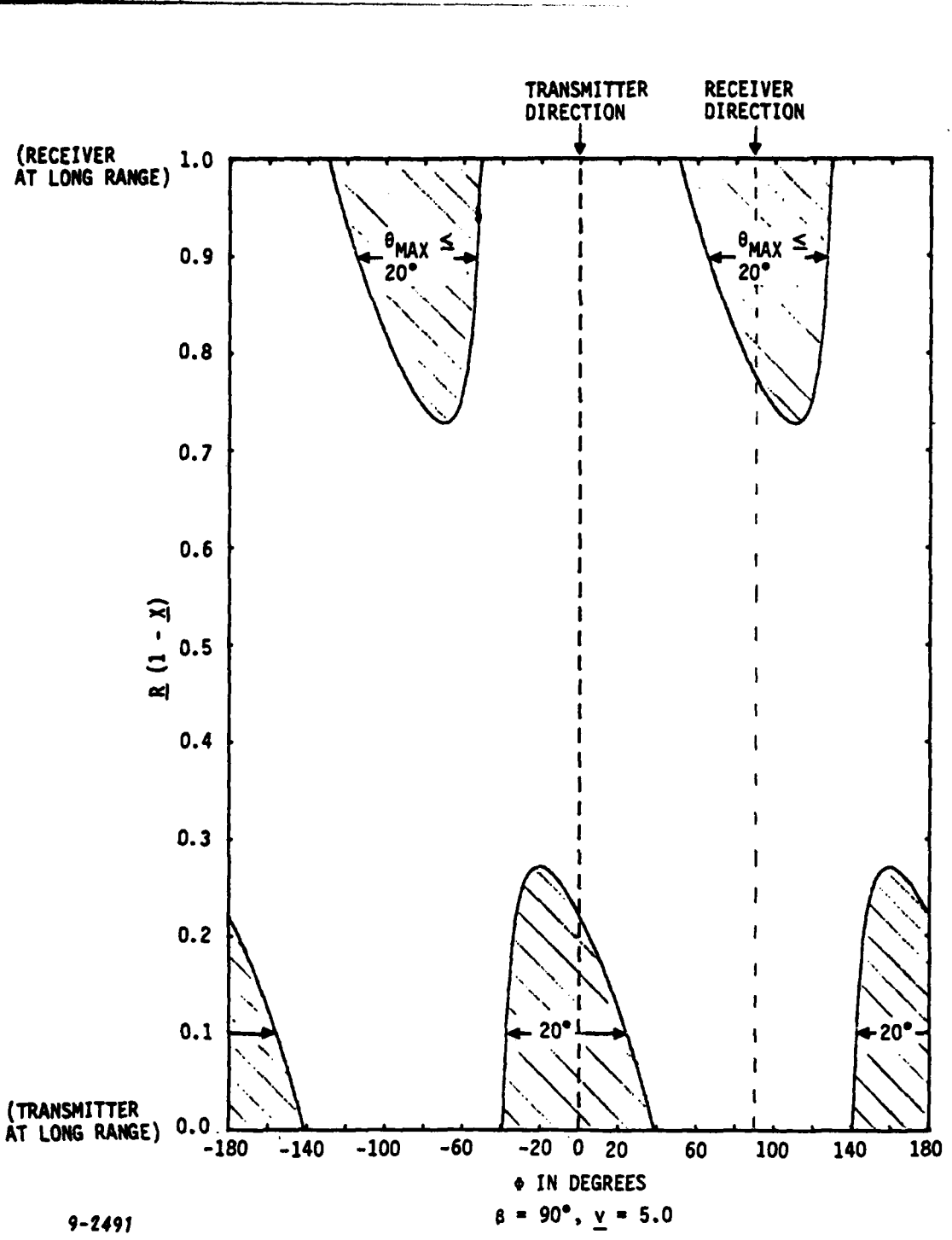

Figure 16. R Versus Φ (Sheet 1 of 7)

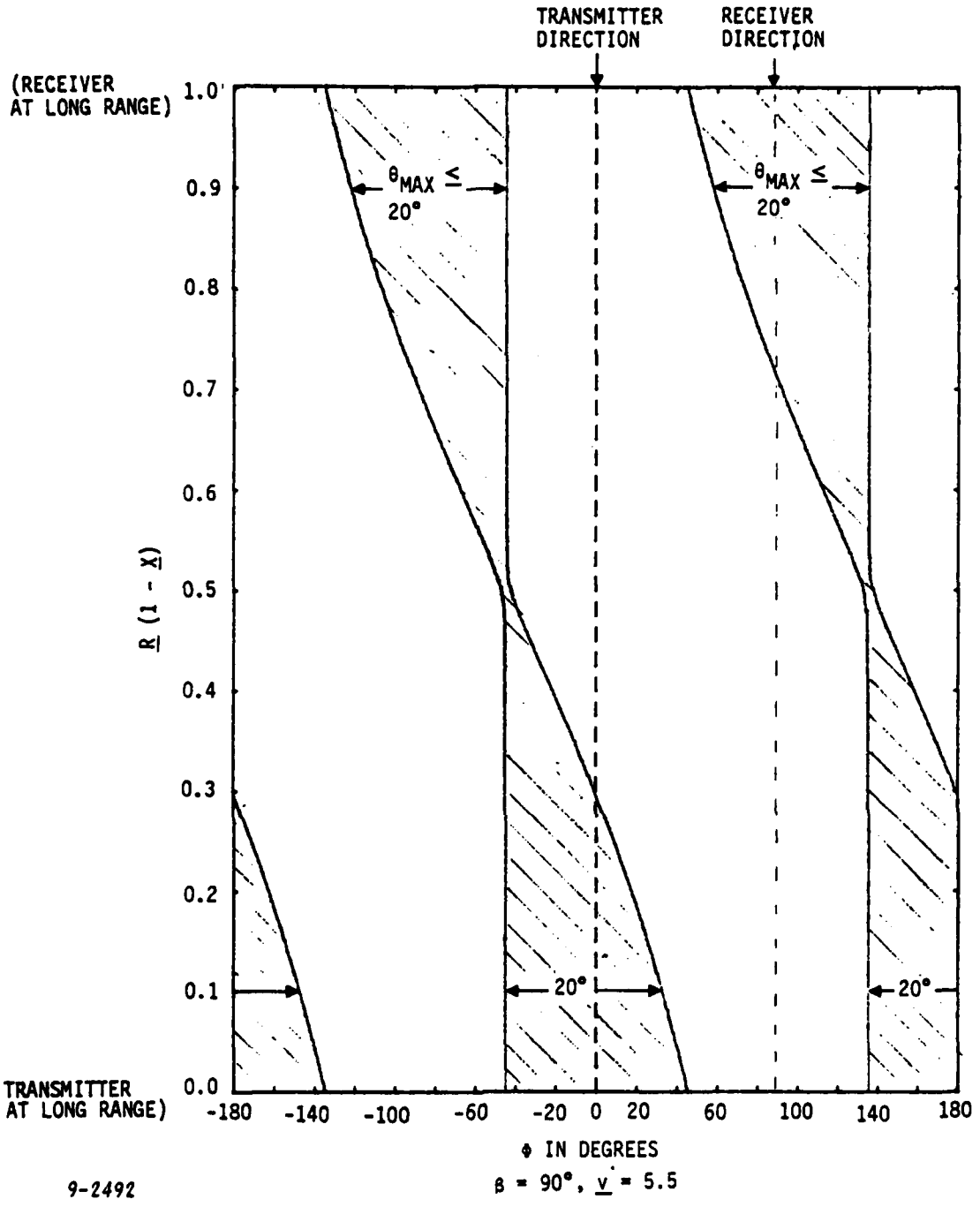

Figure 16. R Versus Φ (Sheet 2 of 7)

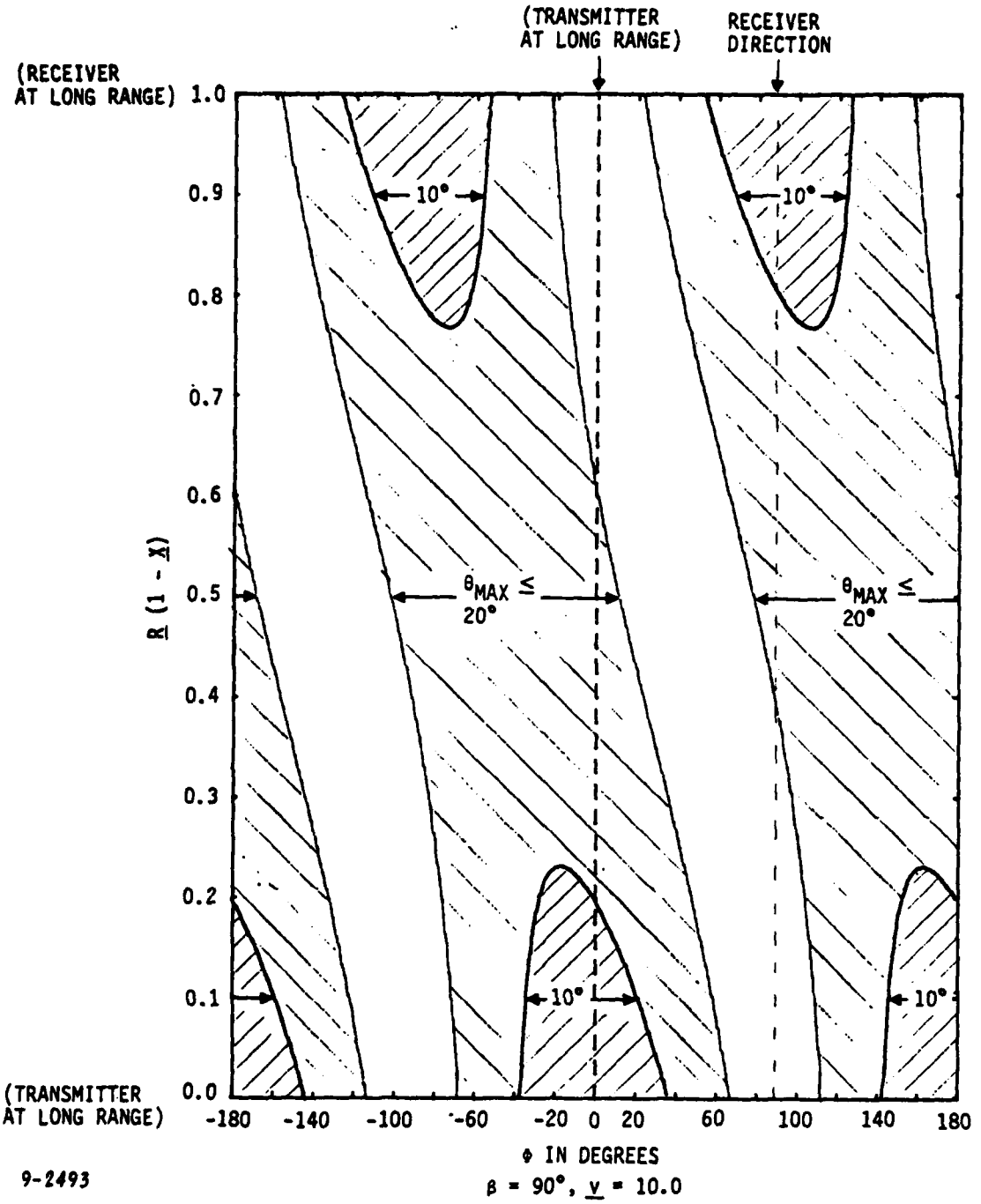

Figure 16. R Versus Φ (Sheet 3 of 7)

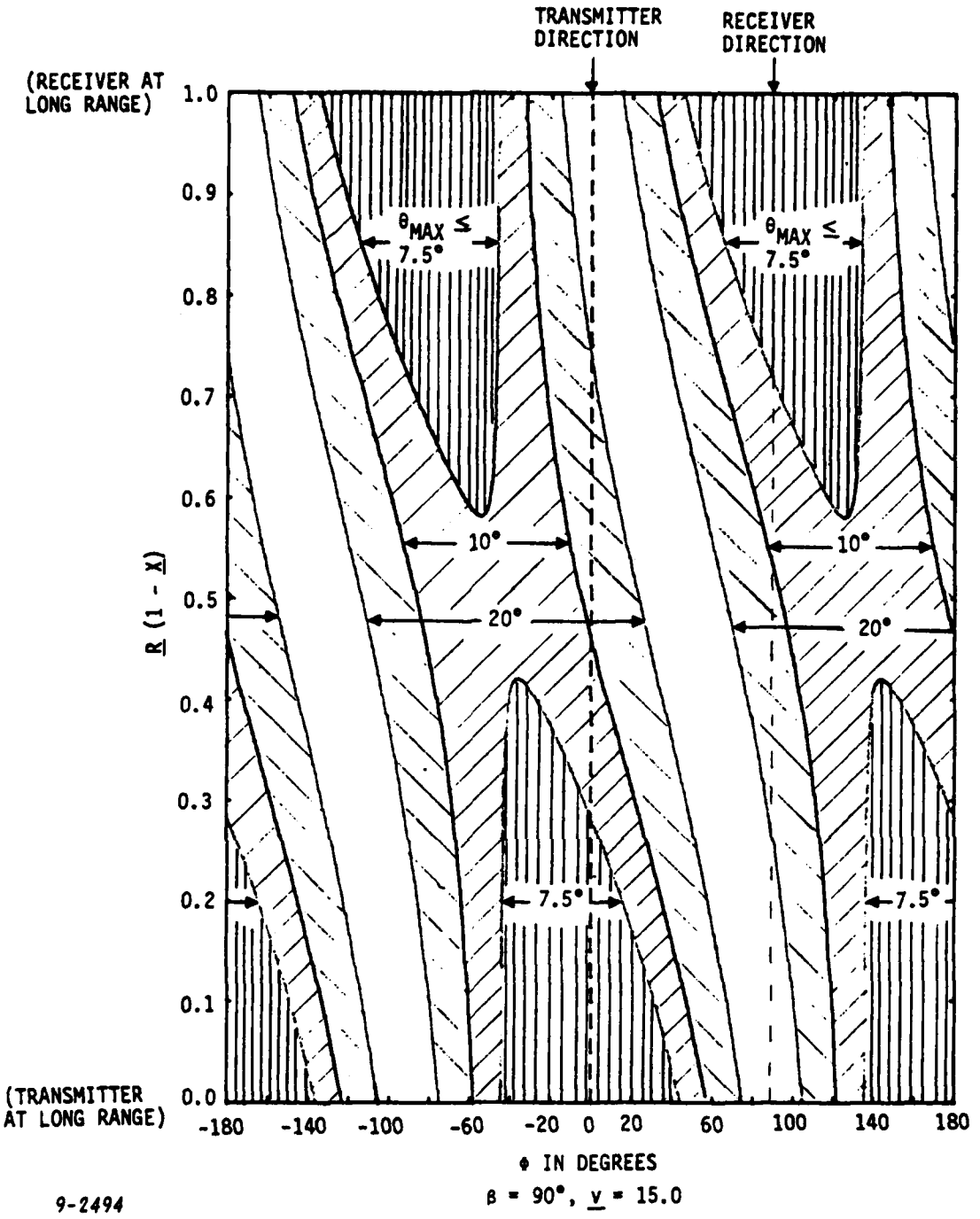

Figure 16. R Versus Φ (Sheet 4 of 7)

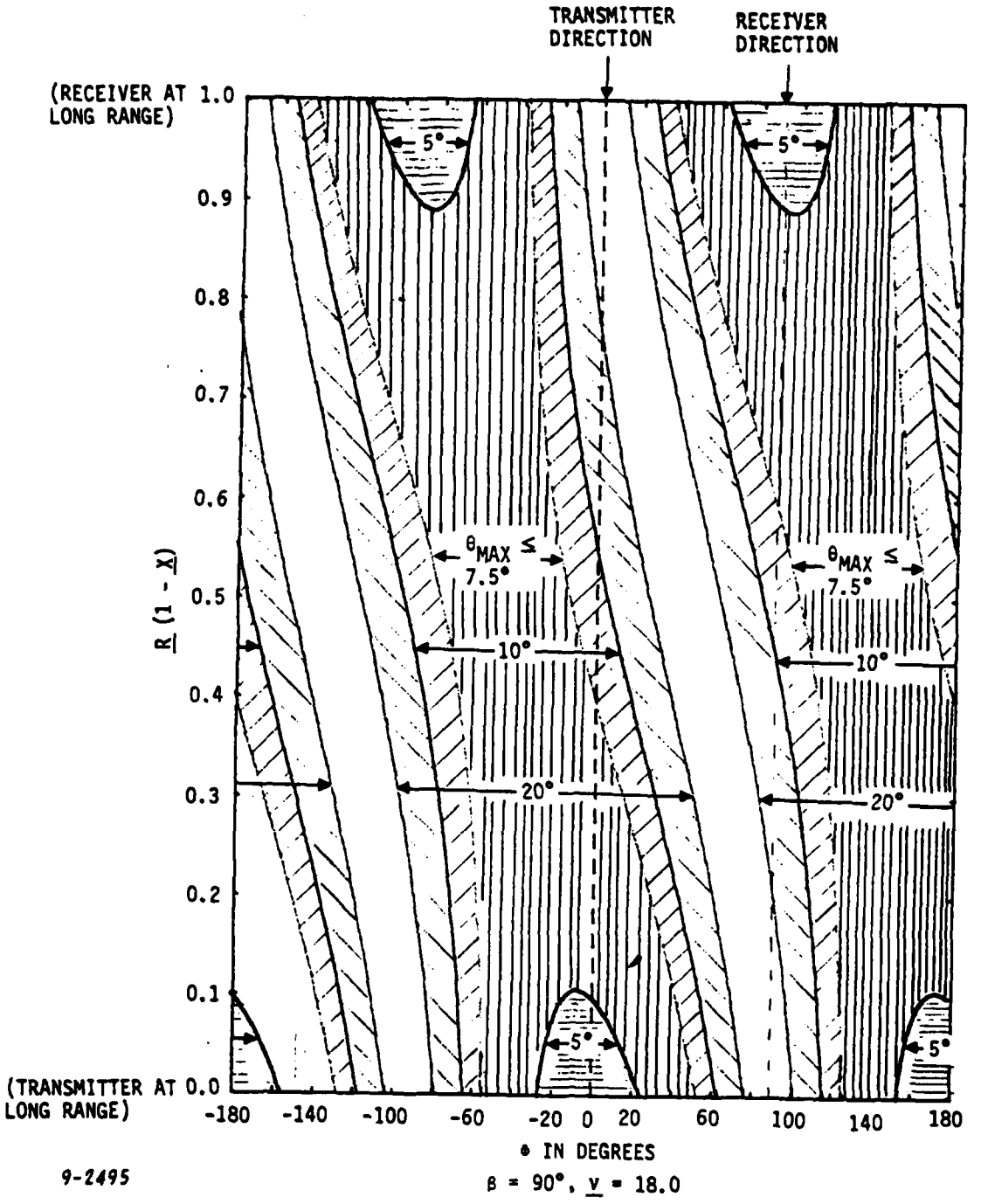

Figure 16. R Versus Φ (Sheet 5 of 7)

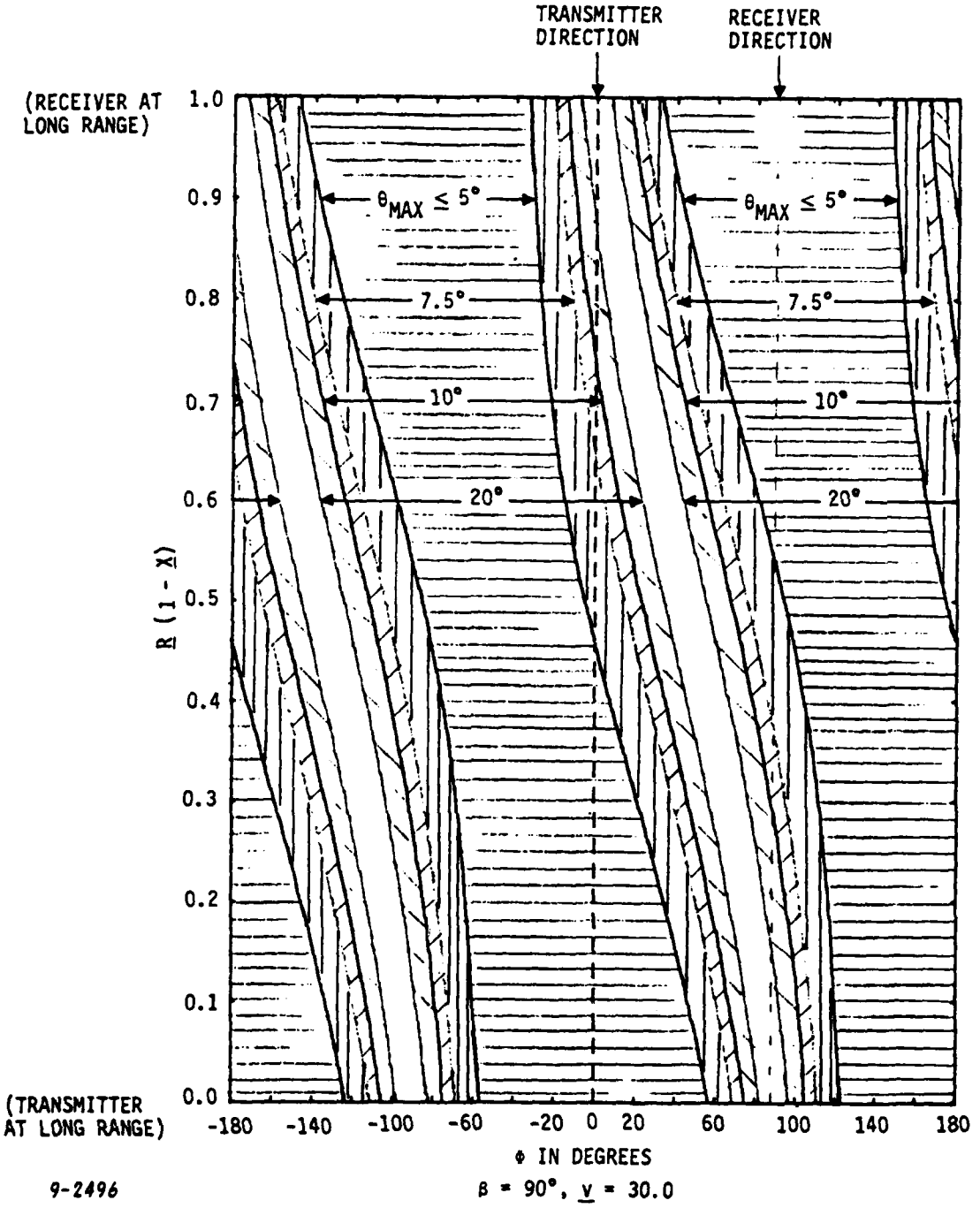

Figure 16. R Versus Φ (Sheet 6 of 7)

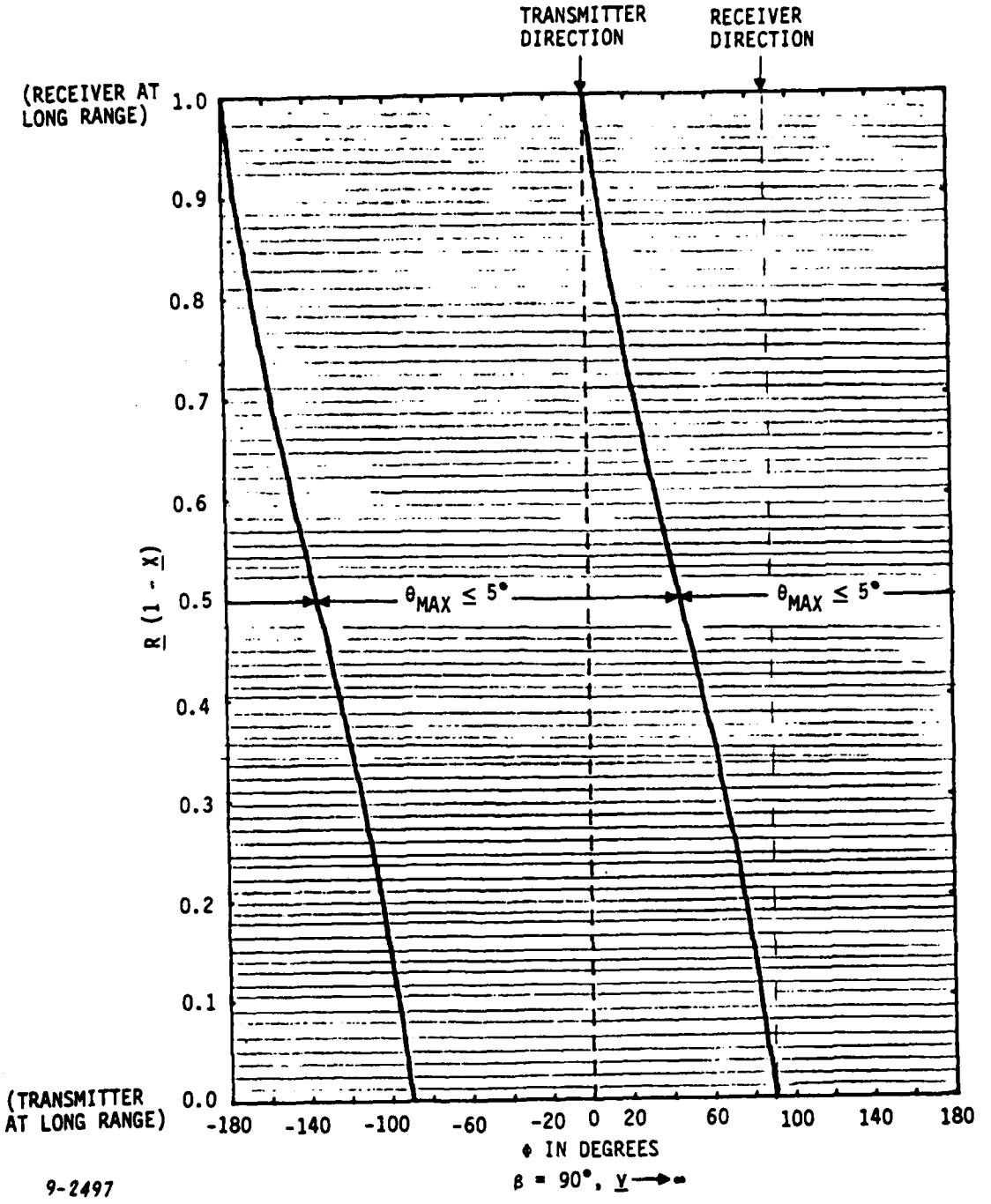

Figure 16. R Versus Φ (Sheet 7 of 7)

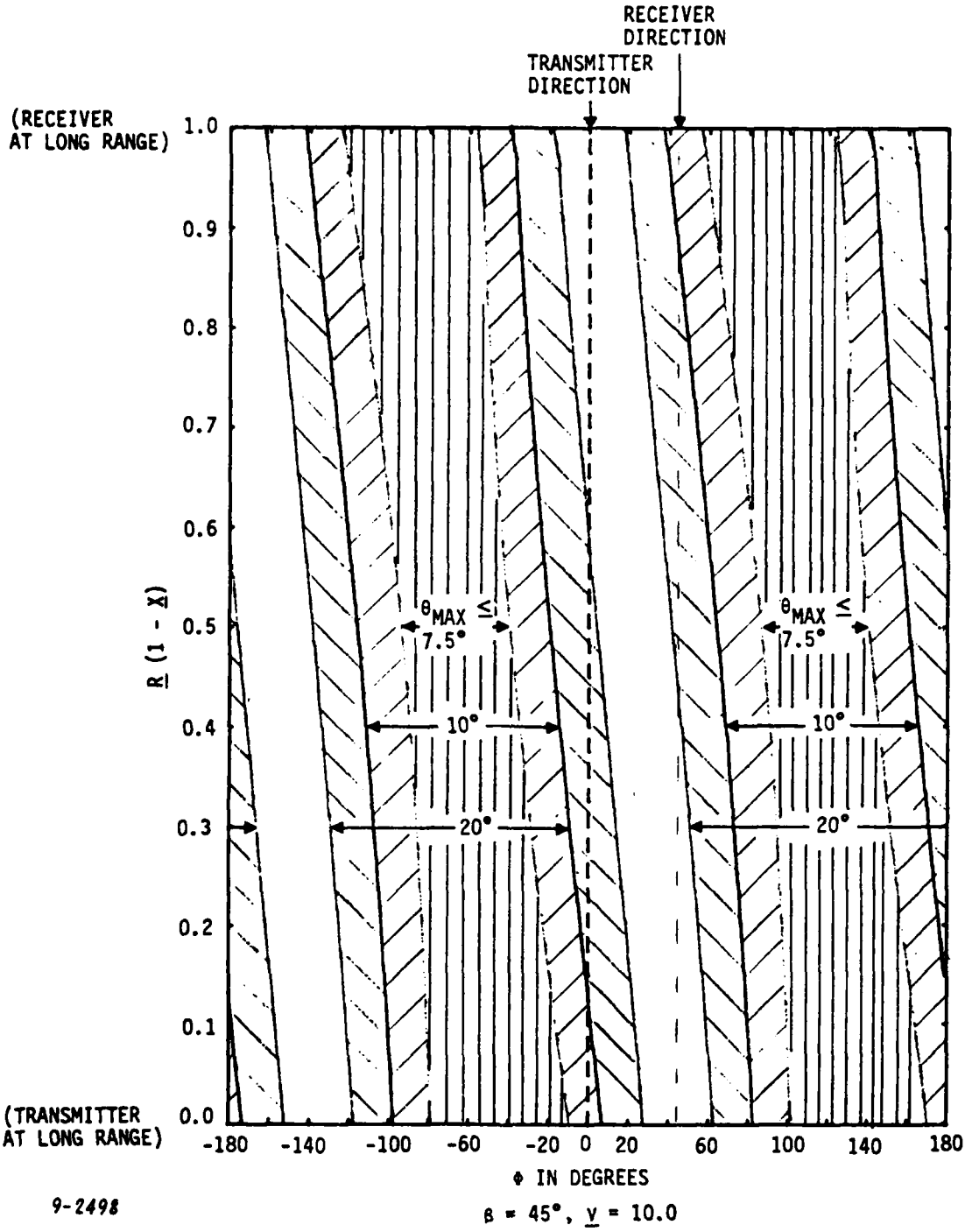

Figure 17. R Versus Φ (Sheet 1 of 2)

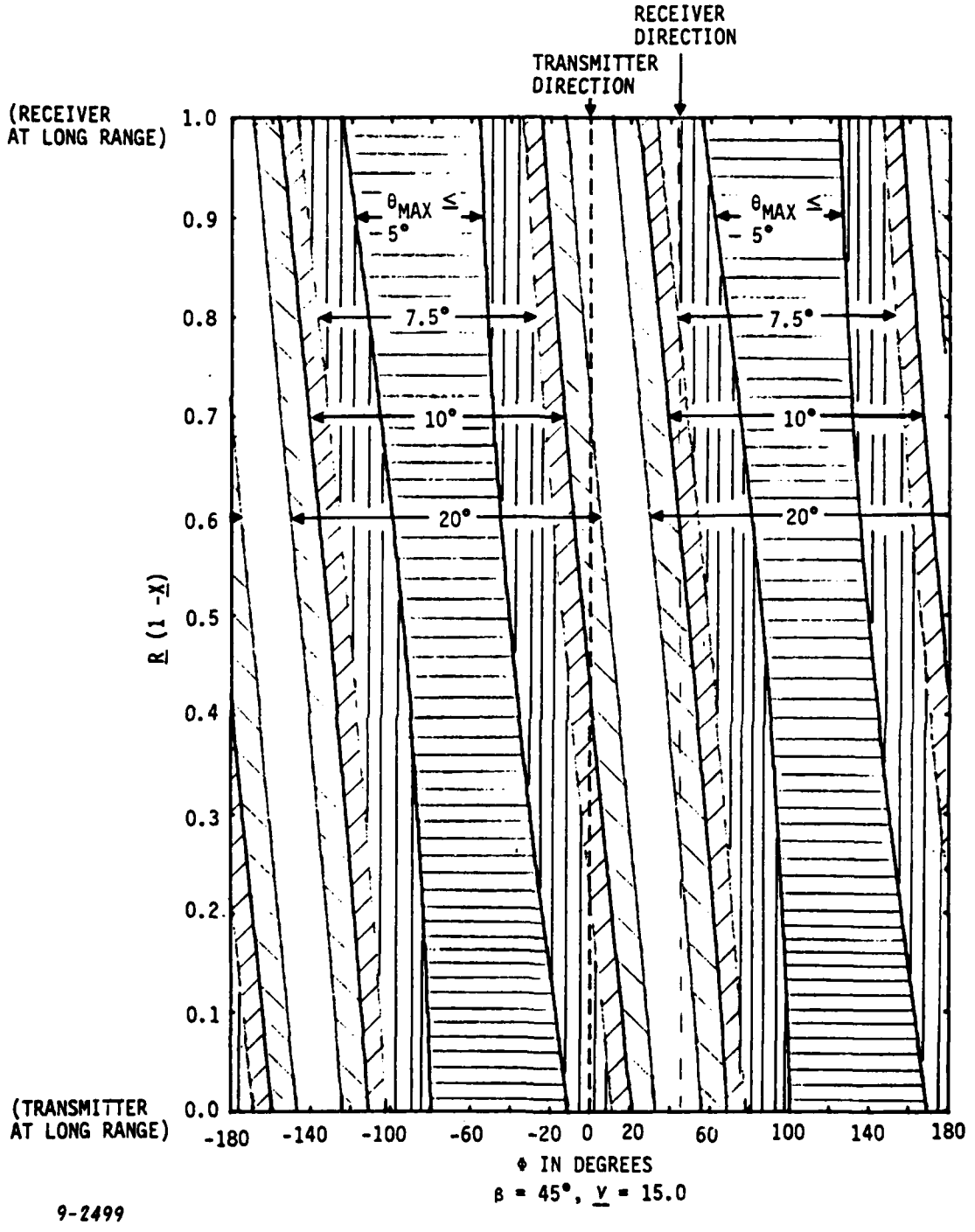

Figure 17. R Versus Φ (Sheet 2 of 2)

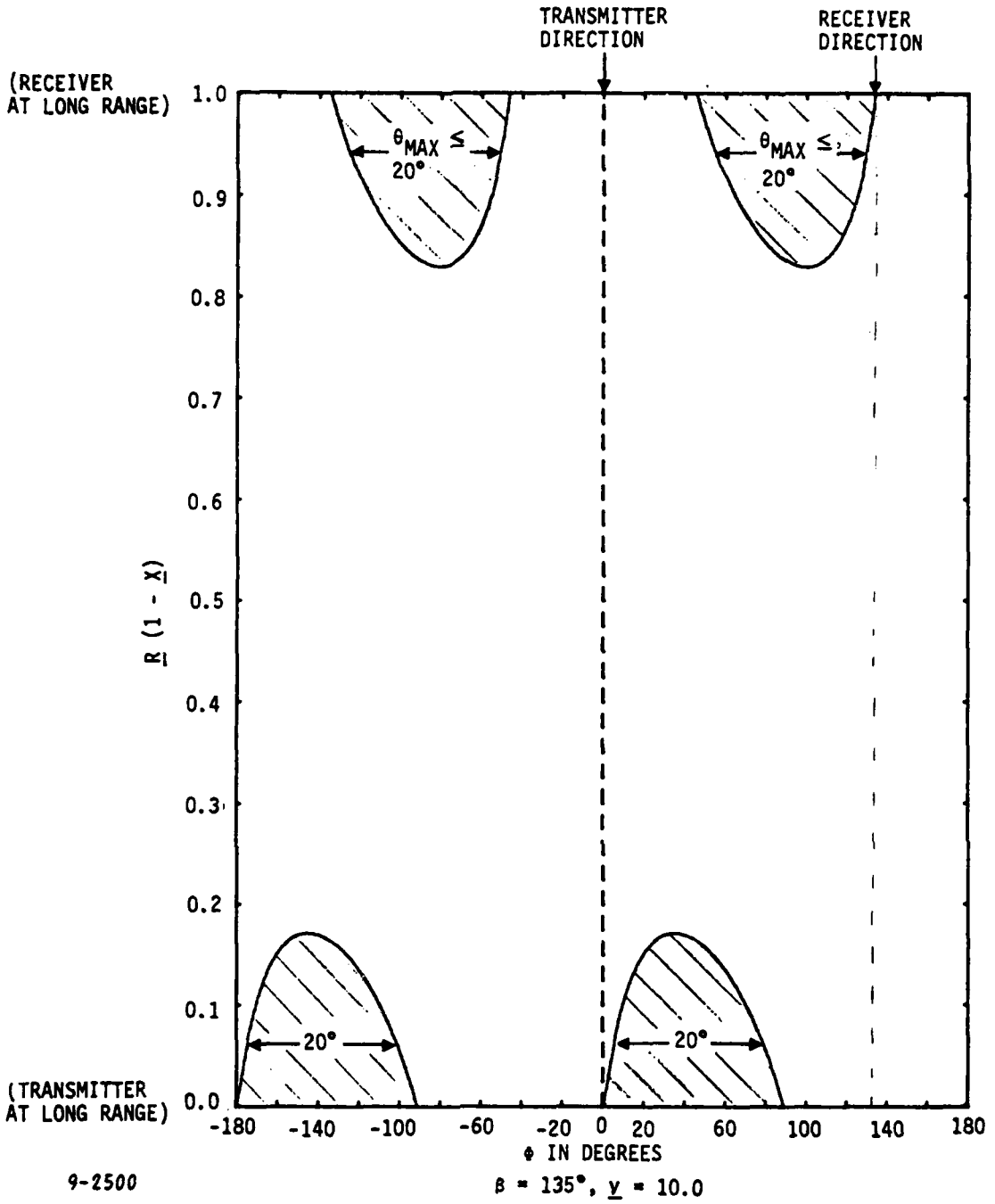

Figure 18. $\underline{R}$ Versus Φ (Sheet 1 of 2)

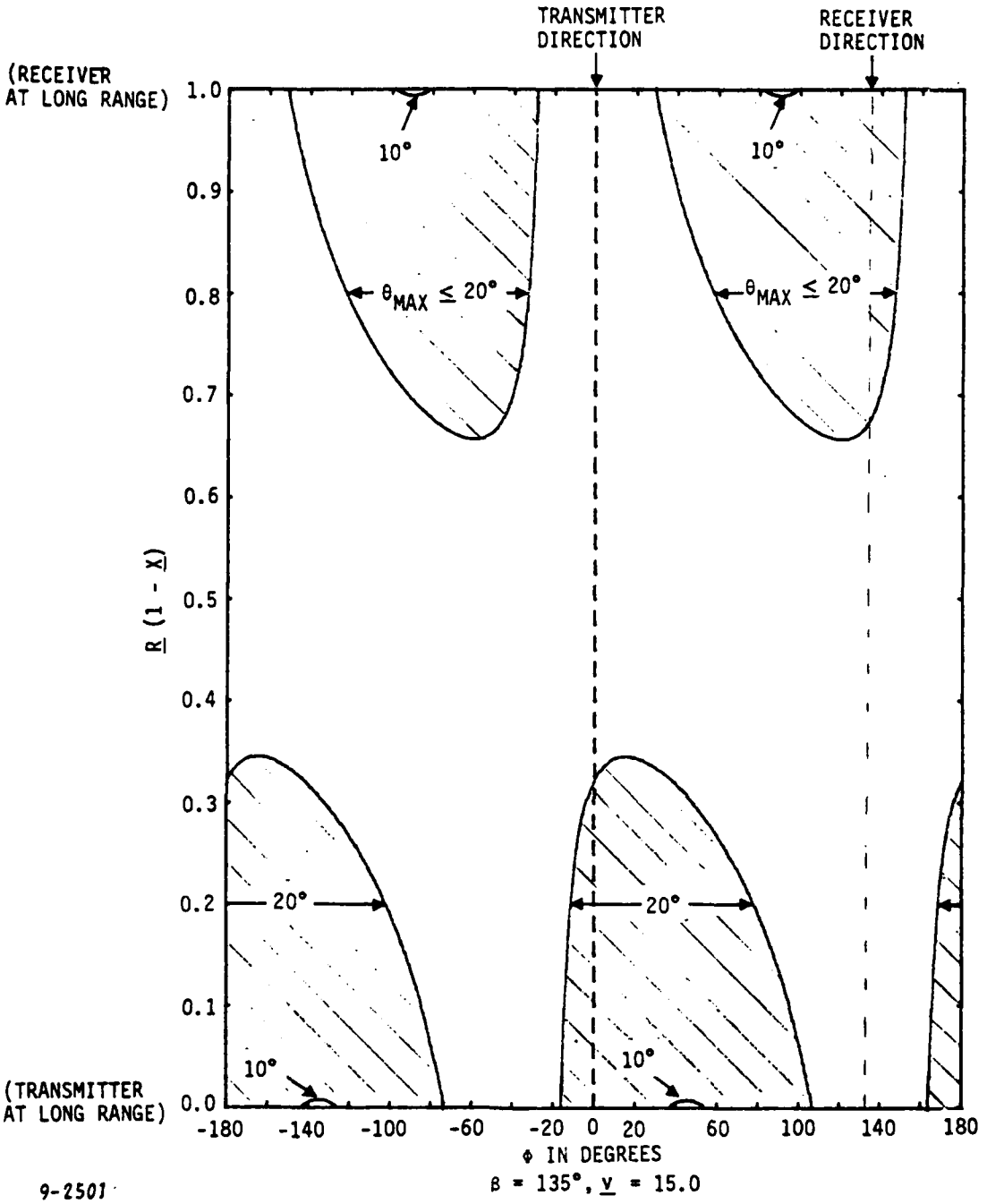

Figure 18. R Versus Φ (Sheet 2 of 2)

The transmitter direction is indicated on Figure 16E by the vertical dashed line drawn at $\Phi = 0$ degree. From Figure 16 the projection of $\underline{v}$ on the fiducial plane is in the same direction as the transmitter for $\Phi = 0$ degree. The receiver direction is indicated on Figure 3-7E and is along the direction of $\Phi = \beta = 90$ degrees.

The vertical scale of Figure 3-7E is labeled $\underline{R}$ and $(1 - \underline{X})$. For $\underline{R} \geq 0.5$, the receiver is at larger range than the transmitter. For $\underline{R} \leq 0.5$, the transmitter is at longer range than the receiver. An example is used to demonstrate the usefulness of the curves.

Consider an imaged aircraft that is 90 miles from the transmitter and 10 miles from the receiver. $\underline{R}$ is then computed as:

$$\underline{R} = \frac{10}{90 + 10} = 0.1$$

The aircraft vertical component of velocity is 30 knots, its horizontal velocity component is 540 knots, and its heading with respect to the transmitter is $\Phi = -20$ degrees. $\underline{v}$ is then computed as:

$$\underline{v} = \frac{540}{30} = 18.0$$

The bistatic angle is $\beta = 90$ degrees. The parameters $\beta = 90$ degrees and $v = 5.0$ prescribe the curve, Figure 16E, be used. From 16E, for $\underline{R} = 0.1$ and $\Phi = -20$ degrees, the image projection tilt will be about 5 degrees. It is important to note that the transmitter and receiver terminals can be switched in locations with the same results.

Examination of Figure 16E with respect to any given condition for θ_{max} shows that the acceptable regions are periodic in Φ and go through two complete cycles. The unhatched portion of the curves indicate that for a given receiver/transmitter/target geometry, a given value of θ_{max} is not necessarily satisfiable.

In viewing the $\underline{R}$ versus Φ curves, if no region is given for which θ_{max} is less than 5 degrees, for example, then this condition cannot be met for that particular engagement geometry.

From Figure 16E, for the curve marked for $\theta_{max} \leq 20$ degrees in the lower right corner of the plot, there appears to be no right-hand arrow marker. Since $\Phi = +180$ degrees is identical to $\Phi = -180$ degrees, the arrow is completed in the lower left-hand corner of the plot at the same value of $\underline{R}$. The boundary of $\Phi = 180$ degrees is continuous with the boundary of $\Phi = -180$ degrees.

It is important to remember that the image projection plane elevation angle is measured with respect to the fiducial plane. The elevation angle can be related to a horizontal plane (of interest for straight and level aircraft flight), if the height of the target is known above a horizontal plane containing the transmitter and receiver and the target ranges to the transmitter and receiver are known.

A survey of Figures 16A through 16G shows the progression of satisfactory regions for θ_{max} for a bistatic angle of 90 degrees and $\underline{v}$ increasing from 5 to ∞ (target motion in the fiducial plane, which is the two-dimentional case). The condition of $\theta_{max} \leq 5$ degrees does not give any appreciable $\underline{R}/\Phi$ areas on the curves until v = 18. At $\underline{v}$ = 5 (Figure 16A), $\theta_{max} \leq 20$ degrees is satisfied for only a small percentage of the plot. With $\underline{v}$ doubled to a value of 10, considerably more conditions of $\underline{R}$ and Φ satisfy $\theta_{max} \leq 20$ degrees. The elevation angle is then very sensitive to $\underline{v}$ or the component of target velocity in the fiducial plane relative to the component normal to the fiducial plane.

The effect of the bistatic angle, β, can be examined by comparing Figures 17A, 16C, and 18A which are all for $\underline{v}$ = 10 but bistatic angles of 45, 90, and 135 degrees, respectively. A comparison of the figures for any value of θ_{max} shows that as β is increased the area for which θ_{max} can be satisfied decreases. A similar comparison of Figures 17B, 16C, and 18B for $\underline{v}$ = 15 also shows a decrease in area with increading β. In general, for a given $\underline{v}$, the area to achieve a maximum θ condition will decrease with increasing β.

An important application of $\underline{R}$ versus Φ tradeoff curves is to aid the system designer in the placement of the transmitter(s) and receiver(s) in a multistatic system. If the expected direction of target aircraft is known within boundaries, then the transmitter(s) and receiver(s) can be placed to minimize the image distortion due to image projection plane tilt. In addition, given target acquisition by a tracking radar and a choice between receiver sites, the receiver site can be chosen to minimize image plane tilt via equation 14 as well as to minimize the expected length of time to collect the synthetic aperture. For reasonable elevation angles (less than 20 degrees), two-dimensional Curl storage referenced to the center of the synthetic aperture can produce an image which is sufficiently geometrically correct to identify the aircraft through pattern recognition.

3.5 CONCLUSIONS

If the orientation of the bistatic image projection plane can be held close in angle to the principal scatterer plane of the target aircraft, then two-dimensional Curl storage/processing can be applied to produce an image which has a high likelihood of being recognized and identified. Curl storage can easily be computed from the radar geometry in the fiducial plane defined at the center of the synthetic aperture.

The orientation of the image projection plane has been expressed as a series of tradeoff curves which can be used to:

- Choose transmitter and receiver site placement.
- Choose a transmitter/receiver combination for a given engagement in the multistatic case.

The elevating angle, θ, of the image projection plane is sensitive to the following parameters with the indicated relationships:

- θ increases with increasing bistatic angle, β
- θ increases with decreasing parameter $\underline{v}$ (the ratio of "horizontal" to "vertical" component of target velocity).

- θ is sensitive to aircraft heading.

The Appendix of this report discusses recommended additional investigations to determine image distortion and resolution limits and investigations into handling those cases which two-dimensional Curl will not produce an image adequate to be identified.

APPENDIX A. GENERAL ANALYSIS

A.1 FOUNDATIONS OF VECTOR ANALYSIS

A.1.1 Two Dimensions (2-D)

The figure below shows a transmitter at ψ_X, receiver at ψ_R, and target at σ direction (and S distance) relative to the field-of-view (FOV) center, in 2-D:

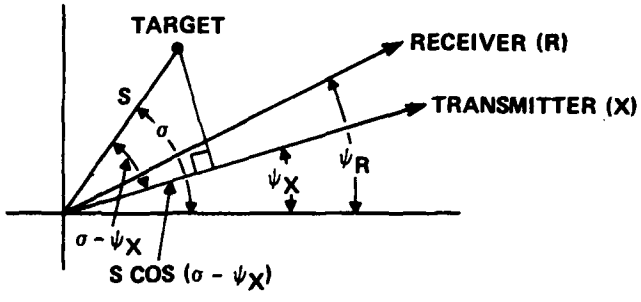

The transmitter and receiver phases ($\phi_{X,R}$) relative to the FOV center are:

$$\phi_X = \frac{2\pi S}{\lambda} \cos(\sigma - \psi_X) \qquad \phi_R = \frac{2\pi S}{\lambda} \cos(\sigma - \psi_R)$$

The total return phase is $\phi = \phi_X + \phi_R$, and return Doppler is:

$$\omega_D = \frac{d}{dt} \phi = \dot{\phi}$$

Using

$$\frac{d}{dt} \cos(\sigma - \psi_i) = \sin(\sigma - \psi_i)\, \dot{\psi}_i$$

$$\omega_D = \frac{2\pi S}{\lambda} \left[\dot{\psi}_X \sin(\sigma - \psi_X) + \dot{\psi}_R \sin(\sigma - \psi_R) \right]$$

Let $\sigma - \psi_i \triangleq \theta_i$ and $\dot{\psi}_i \triangleq \Omega_i$. Then,

$$\omega_D = \frac{2\pi S}{\lambda} \left[\Omega_X \sin\theta_X + \Omega_R \sin\theta_R \right]$$

Drawing Ω_i as vectors perpendicular to the receiver or transmitter directions and in the plane:

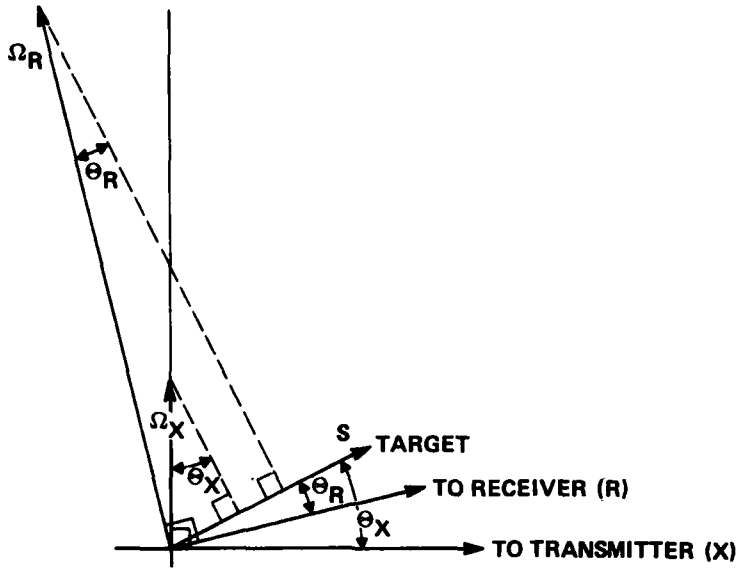

the return Doppler is computed by adding the components of Ω_X and Ω_R in the direction of the target.

Equivalently, Ω_X and Ω_R can be vectorally* added:

$$\bar{\Omega}^T = \bar{\Omega}_X^T + \bar{\Omega}_R^T$$

where the superscript T denotes that the Ω vectors are drawn in the unconventional tangential direction illustrated previously. In Section 3 the symbol ω_T was used instead. Then target Doppler is:

$$\omega_D = \frac{2\pi}{\lambda} \bar{S} \cdot \bar{\Omega}^T = \frac{1}{\lambda} \bar{\Omega}^T \cdot \bar{S}$$

as shown in the next illustration.

---

* Henceforth, a vector is denoted by a bar: $(\bar{A})$, its length by the letter alone: (A), and its direction by a caret $(\hat{A})$, the "unit vector." Scalars have no embelishments: (λ).

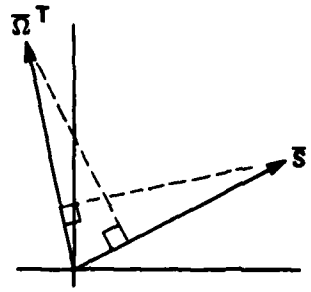

Rotating the coordinates shows that the iso-Dop's are lines perpendicular to Ω, for example: $\bar{\Omega}^T \cdot \bar{S} = \bar{\Omega}^T \cdot \bar{S}'$

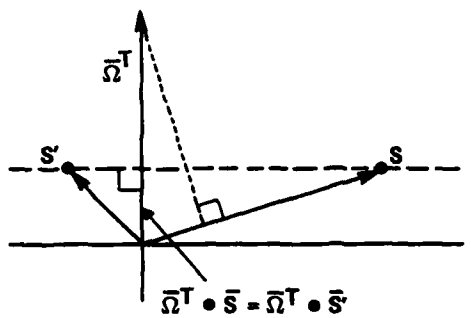

A.1.2 Three Dimensions (3-D)

A solution can be obtained in three dimensions (3-D) by considering the receive and transmit processes separately. Repeating the discussion in paragraph A.1.1; for either the transmitter or receiver using the plane containing the FOV center, target, and either the transmitter or receiver; then:

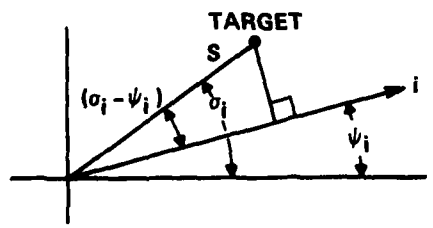

$$\phi_i = \frac{2\pi S}{\lambda} \cos(\sigma_i - \psi_i) \quad \omega_D = \omega_{DX} + \omega_{DR}$$

$$\omega_{Di} = \frac{d}{dt}\ \phi_i = \frac{2\pi S}{\lambda}\ \Omega_i \sin\theta_i$$

Hence,

$$\omega_D = \frac{2\pi S}{\lambda}\ \left[\Omega_X \sin\theta_X + \Omega_R \sin\theta_R\right]$$

as before. However, the transmitter and receiver angles θ_i are no longer in the same plane. The figure and discussion on page 54 still applies; however it must be remembered that Ω_X is in the plane defined by the target, FOV center and transmitter, while Ω_R is in the target, FOV center, receiver plane. $\bar{\Omega}^T$ remains the 3-D vector sum of $\bar{\Omega}_X^T + \bar{\Omega}_R^T$:

$$\omega_D = \frac{2\pi}{\lambda}\ \bar{S} \cdot (\bar{\Omega}_X^T + \bar{\Omega}_R^T) = \frac{2\pi}{\lambda}\ \bar{S} \cdot \bar{\Omega}^T$$

and the iso-Dop's are planes perpendicular to $\bar{\Omega}^T$. Now the surfaces of constant range are planes perpendicular to the bistatic bisector. The intersection of an iso-Dop and an iso-range surface is a line of constant range and Doppler. The image projection plane is defined by (the normal is) any line of constant range and Doppler. Hence, the image projection plane contains $\bar{\Omega}^T$ and the bisector.

A.1.3 2-D Doppler Gradient

Note $\bar{\Omega}^T$ is the Doppler gradient: $\nabla(\bar{S} \cdot \bar{\Omega}^T)$ (for $\bar{\Omega}^T$ a constant and $\bar{S}$ the position vector, customarily called $\bar{r}$) is $\bar{\Omega}^T$. This is proven as follows. Let the x-axis be aligned with $\bar{\Omega}^T$:

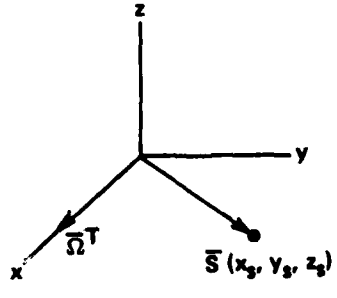

$$\nabla u = \frac{\partial u}{\partial x}\ \hat{x} + \frac{\partial u}{\partial y}\ \hat{y} + \frac{\partial u}{\partial z}\ \hat{z} \text{ by definition}$$

Let $u = \bar{S} \cdot \bar{\Omega}^T = x_s \Omega$

$$\frac{\partial u}{\partial y} = \frac{\partial u}{\partial z} = 0 \qquad \frac{\partial u}{\partial x} = \Omega$$

Therefore

$$\nabla \left(\frac{\lambda \omega_D}{2\pi} \right) = \nabla (\bar{S} \cdot \bar{\Omega}^T) = \Omega \hat{x} = \bar{\Omega}^T \tag{A-1}$$

A.2 VECTOR ANALYSIS

A.2.1 3-D Doppler Gradient

The preceding concepts can be developed generally, using vector analysis. * Consider a rotating rigid body (FOV) and stationary radar.

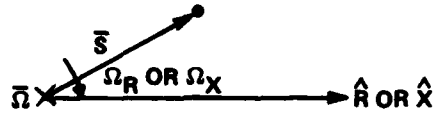

The velocity of the target is $\bar{\Omega} \times \bar{S}$. The component directed toward the receiver or transmitter is:

$$\hat{R} \cdot (\bar{\Omega}_R \times \bar{S}) \text{ or } \hat{X} \cdot (\bar{\Omega}_X \times \bar{S}) \tag{A-2}$$

The Doppler shift is the sum of the receiver directed component with the transmitter directed component:

$$\frac{\lambda \omega_D}{2\pi} = \hat{R} \cdot (\bar{\Omega}_R \times \bar{S}) + \hat{X} \cdot (\bar{\Omega}_X \times \bar{S}) \tag{A-3}$$

The bistatic Doppler gradient is the vector sum of the monostatic gradients:

$$\begin{aligned} \nabla \left(\frac{\lambda \omega_D}{2\pi} \right) &= \nabla \left[\hat{R} \cdot (\bar{\Omega}_R \times \bar{S}) + \hat{X} \cdot (\bar{\Omega}_X \times \bar{S}) \right] \\ &= \nabla \left[\hat{R} \cdot (\bar{\Omega}_R \times \bar{S}) \right] + \nabla \left[\hat{X} \cdot (\bar{\Omega}_X \times \bar{S}) \right] \end{aligned} \tag{A-4}$$

---

* Henceforth all angular velocity vectors are drawn conventionally.

Since

$$\hat{R} \cdot \bar{\Omega}_R \times \bar{S} = \bar{\Omega}_R \cdot \bar{S} \times \hat{R} = \bar{S} \cdot \hat{R} \times \bar{\Omega}_R \text{ (identity)} \tag{A-5}$$

$$\nabla\left(\frac{\lambda\omega_D}{2\pi}\right) = \nabla\left[\bar{S} \cdot \hat{R} \times \bar{\Omega}_R\right] + \nabla\left[\bar{S} \cdot \hat{X} \times \bar{\Omega}_X\right] \tag{A-6}$$

which is the vector sum of the two monostatic gradients. Expanding the gradients (as was done to obtain equation A-1) gives the Doppler gradient:

$$-\nabla\left(\frac{\lambda\omega_D}{2\pi}\right) = \bar{\Omega}_R \times \hat{R} + \bar{\Omega}_X \times \hat{X} \tag{A-7}$$

A.2.2 Range Gradient

To determine the range gradient, let L be the distance from the transmitter to the target to the receiver:

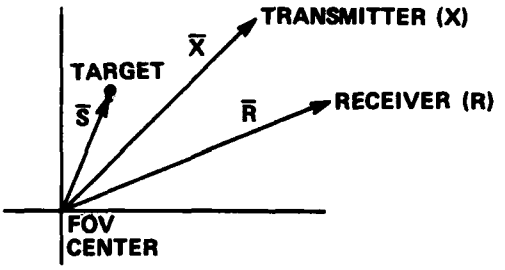

$$L = |\bar{R} - \bar{S}| + |\bar{X} - \bar{S}| \tag{A-8}$$

The range gradient ∇L is:

$$\nabla L = \nabla|\bar{R} - \bar{S}| + \nabla|\bar{X} - \bar{S}| \tag{A-9}$$

Since,

$$|\bar{R} - \bar{S}| \cong R - \bar{S} \cdot \hat{R}$$

$$|\bar{X} - \bar{S}| \cong X - \bar{S} \cdot \hat{X} \tag{A-10}$$

$$\nabla L \cong \nabla R - \nabla\bar{S} \cdot \hat{R} + \nabla X - \nabla\bar{S} \cdot \hat{X} \tag{A-11}$$

Also, since distances R and X are constant, independent of target position:

$$\nabla R = 0 \qquad \nabla X = 0$$

So

$$-\nabla L \cong \nabla \bar{S} \cdot \hat{R} + \nabla \bar{S} \cdot \hat{X} = \hat{R} + \hat{X} \tag{A-12}$$

If the bistatic angle bisector is $\bar{B}$, the range gradient is:

$$-\nabla L \cong \bar{B} = \hat{R} + \hat{X} = (2 \cos \tfrac{\beta}{2})\ \hat{B} \tag{A-13}$$

where β is the bistatic angle between $\hat{X}$ and $\hat{R}$.

A.2.3 Image Plane

Now the normal to the image projection plane, $\bar{N}$, is the vector product of the range and Doppler gradients:*

$$\bar{N} = (\hat{R} + \hat{X}) \times \left[\bar{\Omega}_R \times \hat{R} + \bar{\Omega}_X \times \hat{X}\right] \tag{A-14}$$

Note:

The image projection plane normal can equivalently be obtained from the rotation vector of the bistatic bisector. The equivalence is illustrated below, in two dimensions.

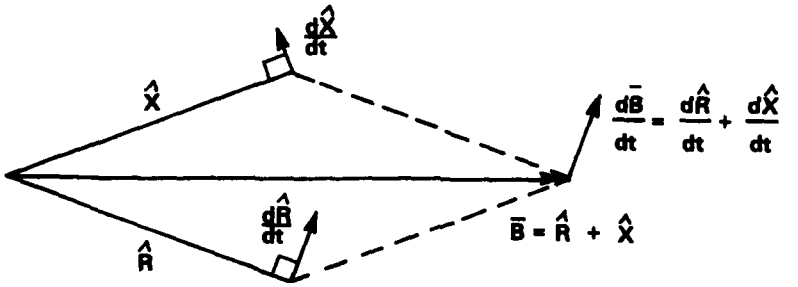

The rotation of the bisector (in three dimensions) can be determined as:

$$\bar{\Omega}_B \triangleq \bar{B} \times \frac{d\bar{B}}{dt} = (\hat{R} + \hat{X}) \times \frac{d\bar{B}}{dt}$$

but

$$\frac{d\bar{B}}{dt} = \frac{d\hat{R}}{dt} + \frac{d\hat{X}}{dt} = \bar{\Omega}_R \times \hat{R} + \bar{\Omega}_X \times \hat{X}$$

and

$$\bar{\Omega}_B = (\hat{R} + \hat{X}) \times \left[\bar{\Omega}_R \times \hat{R} + \bar{\Omega}_X \times \hat{X}\right]$$

Then, from equation A-14 $\bar{N} = \bar{\Omega}_B$

Then, from equation A-14

$$\bar{N} = \bar{\Omega}_B$$

A.2.3.1 Rotating Target Case-Note that if only the target FOV rotates, $\bar{\Omega}_R = \bar{\Omega}_X$ henceforth called $\bar{\Omega}_T$

$$\bar{N} = \bar{B} \times \bar{\Omega}_T \times \bar{B} \tag{A-15}$$

and

$$-\nabla L = \bar{B}$$

$$-\nabla\left(\frac{\lambda \omega_D}{2\pi}\right) = \bar{\Omega}_T \times \bar{B} \tag{A-16}$$

In the monostatic rotating target case $\bar{R} = \bar{X}$

$$-\nabla L = 2\bar{X}$$

$$-\nabla\left(\frac{\lambda \omega_D}{2\pi}\right) = 2\bar{\Omega}_T \times \bar{X}$$

$$\bar{N} = 4\bar{X} \times \bar{\Omega}_T \times \bar{X} \tag{A-17}$$

which are identical to the bistatic gradients and projection plane normal if $\bar{B}$ is replaced by $2\bar{X}$. Further, the Doppler gradient is perpendicular to the range gradient for both bistatic and monostatic imaging of a rotating-only target. Thus, monostatic polar format processing can be used, and identical image projection will be obtained even if the radar is bistatic. These results verify those obtained by Walker[1].

For a rotating target, the image plane tilt is best calculated relative to the rotation axis. From equation A-15:

$$\bar{N} = \bar{B} \times \bar{\Omega}_T \times \bar{B} = (\bar{B} \cdot \bar{B})\,\bar{\Omega}_T - (\bar{B} \cdot \bar{\Omega}_T)\,\bar{B} \text{ (identity)} \tag{A-18}$$

If the scale factor N is of no interest, $\bar{B}$, $\bar{\Omega}_T$ can be replaced with $\hat{B}$, $\hat{\Omega}_T$

$$\bar{N}' = \hat{\Omega}_T - (\hat{B} \cdot \hat{\Omega}_T)\,\hat{B} \tag{A-19}$$

---

[1] J. L. Walker, "Range-Doppler Imaging of Rotating Objects," PhD Thesis; University of Michigan, 1974.

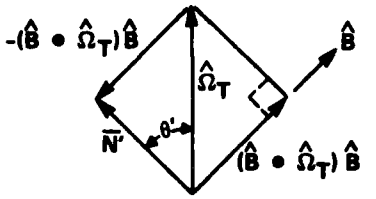

The angle between the image projection plane normal and the rotation axis ($\dot{\theta}$) is 90 degrees, less the angle between $\hat{\Omega}_T$ and $\hat{B}$. Hence, the image projection plane contains $\bar{B}$ and the direction perpendicular to $\bar{B}$ and $\bar{\Omega}_T$ (that is $\bar{B} \times \bar{\Omega}_T$). The projection plane is fixed, and resolution loss is due to target rotation only.

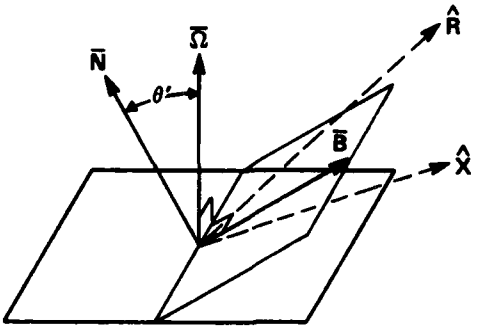

Now the rotation error is $\Omega \sin \dot{\theta}$. The target locus is a circle of radius H sin $\dot{\theta}$. These effects are discussed by Walker for monostatic radar and his analysis can be applied to bistatic radar. The following conclusions may be drawn:

- A 3-D storage system eliminates errors
- 2-D optimum storage requires only timing the receiver to the FOV center range and results in equal error for all target points at the same altitude
- Range and Doppler resolution are both diluted equally by $(1/\cos \dot{\theta})$

Error due to resolution cell (projection plane) motion over a data collection interval Δt is

$$\rho = H \sin \dot{\theta}\, \Omega \Delta t$$

For bistatic radar, the ultimate resolution limited by diffraction of the synthetic aperature is additionally diluted by the bistatic angle:

$$\rho = \frac{\lambda}{2\Omega\Delta t} \times \frac{1}{\cos \dot{\theta}} \times \frac{1}{\cos \beta/2} \qquad \text{(A-20)}$$

Minimum resolution is obtained when: $(\Omega \Delta t)^2 = \frac{\lambda}{H \sin 2\theta' \cos \beta/2}$ and is the greater of (A-21)

$$\rho = \sqrt{\frac{\lambda H \tan \theta'}{2 \cos \beta/2}} \quad \text{or} \quad \frac{\lambda}{\Omega \Delta t \cos \theta' \cos \beta/2} \tag{A-22}$$

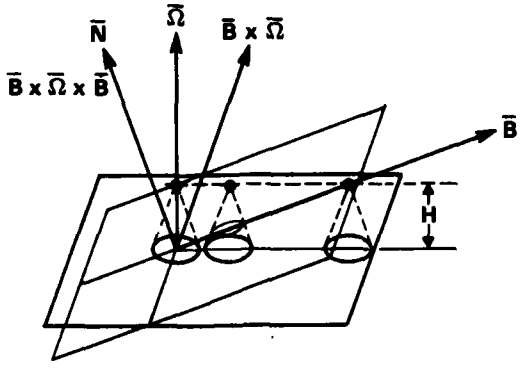

The simple example of a rotating target illuminates the "image projection plane" concept. At any instant, a 3-D object will image as if viewed along $\bar{N}$. If the object is 2-D, parallax is meaningless, and the image will be foreshortened but otherwise the same regardless of $\bar{N}$.

For larger time intervals, the processing can be adjusted to keep points in any one plane fixed. The locus of other points is the projection along $\bar{N}$ to that plane.

For polar processing the one plane is defined by $\bar{\Omega}$. Points on the $\bar{\Omega}$ plane image as points, points off the $\bar{\Omega}$ plane as circles even if they are on the image projection plane. Only the direction $\bar{N}$ is meaningful.

A key question is "Why is the one plane $\bar{\Omega}$?" The answer is that if processing is perfect for the one plane, it must be perfect for any target angle over a full turn of Ω. If the one plane were the projection plane, a particular point on the plane at one instant would be off it at the next instant, hence defocussed.

A.2.3.2 General Case-Returning to the more general case, expanding equation A-14:

$$\bar{N} = \hat{X} \times (\bar{\Omega}_X \times \hat{X}) + \hat{R} \times (\bar{\Omega}_R \times \hat{R}) + \hat{X} \times (\bar{\Omega}_R \times \hat{R}) + \hat{R} \times (\bar{\Omega}_X \times \hat{X}) \tag{A-23}$$

Since for any vectors

$$\bar{U} \times (\bar{V} \times \bar{W}) = (\bar{U} \cdot \bar{W}) \bar{V} - (\bar{U} \cdot \bar{V}) \bar{W} \tag{A-24}$$

$$\hat{U} \times (\bar{V} \times \hat{U}) = (\hat{U} \cdot \hat{U}) \bar{V} - (\hat{U} \cdot \bar{V}) \hat{U} = \bar{V} - (\hat{U} \cdot \bar{V}) \hat{U} \tag{A-25}$$

the components of $\bar{N}$ can be expanded:

$$\hat{X} \times \bar{\Omega}_X \times \hat{X} = \bar{\Omega}_X - (\bar{\Omega}_X \cdot \hat{X})\,\hat{X},\quad \hat{R} \times \bar{\Omega}_R \times \hat{R} = \bar{\Omega}_R - (\bar{\Omega}_R \cdot \hat{R})\,\hat{R}$$

$$\hat{X} \times \bar{\Omega}_R \times \hat{R} = (\hat{X} \cdot \hat{R})\,\bar{\Omega}_R - (\hat{X} \cdot \bar{\Omega}_R)\,\hat{R} = \cos\beta\,\bar{\Omega}_R - (\hat{X} \cdot \bar{\Omega}_R)\,\hat{R}$$

$$\hat{R} \times \bar{\Omega}_X \times \hat{X} = (\hat{X} \cdot \hat{R})\,\bar{\Omega}_X - (\hat{R} \cdot \bar{\Omega}_X)\,\hat{X} = \cos\beta\,\bar{\Omega}_X - (\hat{R} \cdot \bar{\Omega}_X)\,\hat{X} \qquad \text{(A-26)}$$

Then:

$$\boxed{\bar{N} = (1 + \cos\beta)\,(\bar{\Omega}_R + \bar{\Omega}_X) - \left[\bar{\Omega}_R \cdot (\hat{R} + \hat{X})\right]\hat{R} - \left[\bar{\Omega}_X \cdot (\hat{R} + \hat{X})\right]\hat{X}} \qquad \text{(A-27)}$$

Equation A-27 is a general expression for the direction of the image projection plane, given the transmitter ($\hat{X}$) and receiver ($\hat{R}$) directions, and the apparent target rotations as seen from the transmitter ($\bar{\Omega}_X$) and receiver ($\bar{\Omega}_R$). The apparent rotation can be the result of target rotation or translation; or radar translation; or any combination.

A.2.3.3 Translating Target Case-In a desire to simplify equation A-27 further, special cases are considered. The elementary target-only rotation case has already been examined, and shown to reduce to the monostatic rotating target case. Now the case of translation only; of target, receiver or transmitter, or any combination will be considered. The expression in equation A-27 or A-14 can be used directly, however, in this case, a simpler expression can be obtained by calculating the orientation of the projection plane relative to a "tilted reference plane" defined as containing the target, receiver and transmitter. This reference plane has greater physical significance than the horizontal (or ground), since gravity plays no part in the imaging process. This choice of a reference plane is analogous to the choice of the axis of rotation as a reference for the rotating target case.

Now, from the definition of a scalar product

$$\hat{N} \cdot \hat{R} \times \hat{X} = \cos\theta \sin\beta \qquad \text{(A-28)}$$

where θ is the image plane tilt relative to the reference plane $\hat{R} \times \hat{X}$. Applying equation A-28 to equation A-27:

$$N \sin\beta \cos\theta = \bar{N} \cdot (\hat{R} \times \hat{X}) = (1 + \cos\beta)\,(\bar{\Omega}_X + \bar{\Omega}_R) \cdot (\hat{R} \times \hat{X}) -$$

$$(\bar{B} \cdot \bar{\Omega}_R)\,\hat{R} \cdot (\hat{R} \times \hat{X}) - (\bar{B} \cdot \bar{\Omega}_X)\,\hat{X} \cdot (\hat{R} \times \hat{X}) \qquad \text{(A-29)}$$

Using an identity, and the fact that the vector product of any vector with itself is zero:

$$\hat{R} \cdot \hat{R} \times \hat{X} = \hat{X} \cdot \hat{R} \times \hat{R} = 0,\quad \hat{X} \cdot \hat{R} \times \hat{X} = \hat{R} \cdot \hat{X} \times \hat{X} = 0$$

Then

$$N \sin \beta \cos \theta = (\bar{\Omega}_X + \bar{\Omega}_R) \cdot (\hat{R} \times \hat{X}) (1 + \cos \beta) \tag{A-30}$$

Likewise from the definition of a vector product:

$$|\bar{U} \times \bar{V}| = UV \sin \gamma$$

where $\bar{U}$ and $\bar{V}$ are any vectors, and γ is the angle between them. The axis of rotation of γ is the direction of $\bar{U} \times \bar{V}$. Then:

$$N \sin \beta \sin \theta = |\bar{N} \times (\hat{R} \times \hat{X})| = |(1 + \cos \beta) (\bar{\Omega}_R + \bar{\Omega}_X) \times (\hat{R} \times \hat{X}) - (\bar{B} \cdot \bar{\Omega}_R) \hat{R} \times (\hat{R} \times \hat{X}) - (\bar{B} \cdot \bar{\Omega}_X) \hat{X} \times (\hat{R} \times \hat{X})| \tag{A-31}$$

Expanding equation A-31:

$$N \sin \beta \sin \theta = |(1 + \cos \beta) \left[\bar{\Omega}_R \times (\hat{R} \times \hat{X}) + \bar{\Omega}_X \times (\hat{R} \times \hat{X}) \right] - (\bar{\Omega}_R \cdot \bar{B}) \hat{R} \times (\hat{R} \times \hat{X}) - (\bar{\Omega}_X \cdot \bar{B}) \hat{X} \times (\hat{R} \times \hat{X})| \tag{A-32}$$

Then expanding the triple vector products using identity (equation A-24):

$$N \sin \beta \sin \theta = \Big|(1 + \cos \beta) \left[(\bar{\Omega}_R \cdot \hat{X}) \hat{R} - (\bar{\Omega}_R \cdot \hat{R}) \hat{X} + (\bar{\Omega}_X \cdot \hat{X}) \hat{R} - (\bar{\Omega}_X \cdot \hat{R}) \hat{X} \right] - (\bar{\Omega}_R \cdot \bar{B}) \left[(\hat{R} \cdot \hat{X}) \hat{R} - (\hat{R} \cdot \hat{R}) \hat{X} \right] - (\bar{\Omega}_X \cdot \bar{B}) \left[(\hat{X} \cdot \hat{X}) \hat{R} - (\hat{X} \cdot \hat{R}) \hat{X} \right] \Big| \tag{A-33}$$

Substituting

$$\hat{X} \cdot \hat{X} = 1 = \hat{R} \cdot \hat{R} \tag{A-34}$$

and

$$\hat{X} \cdot \hat{R} = \cos \beta$$

Then collecting terms, equation A-33 simplifies to

$$N \sin \beta \sin \theta = \left| \left[\bar{\Omega}_R \cdot \hat{X} - \bar{\Omega}_X \cdot \hat{R} + (\cos \beta) (\bar{\Omega}_X \cdot \hat{X} - \bar{\Omega}_R \cdot \hat{R}) \right] (\hat{R} + \hat{X}) \right| \tag{A-36}$$

Dividing equation A-36 by equation A-30 gives:

$$\tan \theta = \left| \frac{\bar{\Omega}_R \cdot \hat{X} - \bar{\Omega}_X \cdot \hat{R} + \cos \beta \, (\bar{\Omega}_X \cdot \hat{X} - \bar{\Omega}_R \cdot \hat{R})}{(\bar{\Omega}_X + \bar{\Omega}_R) \cdot (\hat{R} \times \hat{X}) \cos \beta/2} \hat{B} \right| \tag{A-37}$$

The denominator clearly depends only upon the components of the rotation vectors normal to the reference plane. The numerator in fact depends only upon the component of transmitter rotation perpendicular to the transmitter direction, and the component of receiver rotation perpendicular to the receiver direction, which can be verified by examining equation A-14 from which equation A-36 was obtained. Thus, the image projection plane orientation does not depend upon whether or not the target is rotating. However, if the target is not rotating:

$$\bar{\Omega}_X \cdot \dot{\hat{X}} = O \qquad \bar{\Omega}_R \cdot \dot{\hat{R}} = O \tag{A-38}$$

and equation A-37 simplifies to:

$$\boxed{\tan \theta = \left| \frac{\bar{\Omega}_R \cdot \hat{X} - \bar{\Omega}_X \cdot \hat{R}}{(\bar{\Omega}_X + \bar{\Omega}_R) \cdot (\hat{R} \times \hat{X}) \cos \beta/2} \hat{B} \right|} \tag{A-39}$$

as the image plane tilt angle θ relative to the target/transmitter/receiver reference plane when the target, transmitter and receiver are translating. This means that tilt angle magnitude is the arctangent of the scalar fraction, and the axis of tilt is the bistatic bisector direction $\hat{B}$. This result is explored in paragraph 3.3 under the further restriction that only the target translates, or equivalently that the velocities of the transmitter and receiver relative to the target are identical.

For a target translating at velocity $\bar{v}$, and both receiver and transmitter stationary:

$$\bar{\Omega}_R = \frac{\hat{R} \times \bar{v}}{R} \qquad \bar{\Omega}_X = \frac{\hat{X} \times \bar{v}}{X} \tag{A-40}$$

Then equation A-39 becomes

$$\tan \theta = \frac{\dfrac{\hat{R} \times \bar{v} \cdot \hat{X}}{R} - \dfrac{\hat{X} \times \bar{v} \cdot \hat{R}}{X}}{\cos \beta \left(\dfrac{\hat{R} \times \bar{v}}{R} + \dfrac{\hat{X} \times \bar{v}}{X} \right) \cdot (\hat{R} \times \hat{X})} \tag{A-41}$$

$$\tan \theta \cos \beta = \frac{X (\hat{R} \times \bar{v} \cdot \hat{X}) - R (\hat{X} \times \bar{v} \cdot \hat{R})}{X (\hat{R} \times \bar{v}) \cdot (\hat{R} \times \hat{X}) + R (\hat{X} \times \bar{v}) \cdot (\hat{R} \times \hat{X})} \tag{A-42}$$

Since

$$\bar{U} \cdot \bar{V} \times \bar{W} = \bar{V} \cdot \bar{W} \times \bar{U} \text{ (identity)} \tag{A-43}$$

$$\tan e \cos \beta = \frac{X (\bar{v} \cdot \dot{\hat{X}} \times \hat{R}) - R (\bar{v} \cdot \hat{R} \times \dot{\hat{X}})}{X (\hat{R} \times \bar{v}) \cdot (\hat{R} \times \dot{\hat{X}}) + R (\dot{\hat{X}} \times \bar{v}) \cdot (\hat{R} \times \dot{\hat{X}})} \tag{A-44}$$

As in Section 3, defining the x, y plane so x is aligned with $\hat{X}$ and y is in the same plane as $\hat{R}$ and $\dot{\hat{X}}$

$$\tan e \cos \beta = \frac{X v_z \sin \beta + R v_z \sin \beta}{X (\hat{R} \times \bar{v}) \cdot (\hat{R} \times \dot{\hat{X}}) + R (\dot{\hat{X}} \times \bar{v}) \cdot (\hat{R} \times \dot{\hat{X}})} \tag{A-45}$$

where v_x, v_y, v_z are the components of $\bar{v}$. Since

$$(\bar{T} \times \bar{U}) \cdot (\bar{V} \times \bar{W}) = (\bar{T} \cdot \bar{V}) (\bar{U} \cdot \bar{W}) - (\bar{T} \cdot \bar{W}) (\bar{U} \cdot \bar{V}) \text{ (identity)} \tag{A-46}$$

$$X (\hat{R} \times \bar{v}) \cdot (\hat{R} \times \dot{\hat{X}}) = X \bar{v} \cdot \dot{\hat{X}} - X (\hat{R} \cdot \dot{\hat{X}}) (\bar{v} \cdot \hat{R})$$

$$= X v_x - X \cos \beta \, (\bar{v} \cdot \hat{R}) \tag{A-47}$$

$$R (\dot{\hat{X}} \times \bar{v}) \cdot (\hat{R} \times \dot{\hat{X}}) = R (\hat{R} \cdot \dot{\hat{X}}) (\bar{v} \cdot \dot{\hat{X}}) - R \bar{v} \cdot \hat{R}$$

$$= R \cos \beta \, v_x - R \bar{v} \cdot \hat{R} \tag{A-48}$$

where

$$\bar{v} \cdot \hat{R} = v_y \sin \beta + v_x \cos \beta \tag{A-49}$$

Then the denominator of equation A-44 becomes

$$X v_x (1 - \cos^2 \beta) - X v_y \sin \beta \cos \beta - R v_z \sin \beta = \sin \beta \Big(X v_x \sin \beta - X v_y \cos \beta - R v_y \Big) \tag{A-50}$$

Hence

$$\tan e = \frac{v_z (X + R)}{\cos \beta \left[X \left(v_x \sin \beta - v_y \cos \beta \right) - R v_z \right]} \tag{A-51}$$

Equation A-51 is identical to equation 11 (paragraph 3.4.2.3) which was derived in a slightly different fashion.

MISSION
of
Rome Air Development Center

RADC plans and executes research, development, test and selected acquisition programs in support of Command, Control Communications and Intelligence (C^3I) activities. Technical and engineering support within areas of technical competence is provided to ESD Program Offices (POs) and other ESD elements. The principal technical mission areas are communications, electromagnetic guidance and control, surveillance of ground and aerospace objects, intelligence data collection and handling, information system technology, ionospheric propagation, solid state sciences, microwave physics and electronic reliability, maintainability and compatibility.

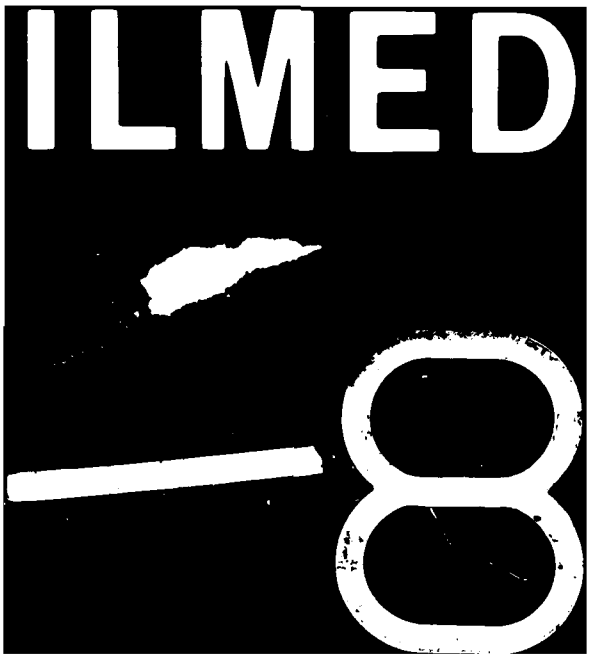
ILMED
8